MIT Academy of Engineering, Alandi(D)

Proceedings of the

7th National Conference On

Multidisciplinary Research in Science and Engineering (NCMRSE)

"विज्ञान व प्रौद्योगिकी में बहुविषयी अनुसंधान"

ISBN: 978-93-84659-59-2

3 & 4 June 2016

Department of Engineering Sciences
MIT Academy of Engineering,
Alandi (D) , Pune - 412105,
Maharashtra, India.

An Autonomous Institute affiliated to SPPU, Pune

Website :- www.mitaoe.ac.in

International E – Publication

www.isca.me ,www.isca.co.in

International E - Publication

427, Palhar Nagar, RAPTC, VIP-Road, Indore-452005 (MP) INDIA

Phone: +91-731-2616100, Mobile: +91-80570-83382 E-mail: **contact@isca.co.in**, Website:**www.isca.me** , **www.isca.co.in**

7th National Conference on Multidisciplinary Research in Science and Engineering (NCMRSE)-2016, 3rd-4th June, 2016

Organised by:

MIT Academy of Engineering,

Alandi (D), Pune-412105

ISBN: 978-93-84659-59-2

CONTENTS

Proceedings of 7th National Conference on Multidisciplinary Research in Science & Engineering, MIT AOE Alandi, Pune, 3-4 June 2016 ,pp. 1-8, ISBN: 978-93-84659-59-2

EXPERIMENTAL INVESTIGATIONS ON ENERGY ABSORPTION CHARACTERISTICS OF SYNTACTIC FOAM-CORED SANDWICH COMPOSITES

Rajnitu Rakshaskar
VPM's Maharshi Parashuram College of Engineering, Velneshwar, Maharashtra, India

Abstract

Syntactic foams are composite materials synthesized by dispersing hollow microspheres in a polymeric matrix. Syntactic foams have gained immense importance as a lightweight and damage-tolerant material when used in foam-cored sandwich structures. This work focuses on the energy absorption capability of three different types of syntactic foam-cored sandwich structures. The main difference between three types of syntactic foam-cores was the type of resin impregnated paper honeycomb structure infused in it. The structure developed from Nomex paper and Kraft paper. Developed foams cores were additionally strengthened by providing E-glass/epoxy face-sheets. Sandwich composites were then conditioned before being cut to required dimensions as per ASTM standard. Sandwich composite coupons were subjected to low-velocity impact test using an Instron Dynatup 8250 drop weight impact testing machine at two different energy levels. Impact responses such as peak impact load, energy absorption and damage modes were evaluated in terms of core stiffness of sandwich structures. Also, a dimensionless parameter - ductility index was evaluated, which is found useful for ranking the impact performance of different sandwich composite under similar testing conditions. Results of the study indicate that, with the infusion of resin impregnated paper honeycomb structure in syntactic foam-cored sandwich composites, the resistance to damage initiation and propagation has improved. Energy is dissipated primarily through damage initiation and then through damage propagation. The improved energy dissipation characteristics of the stiffened syntactic foam-cored sandwich composite promise its applications in stiffness critical safety structures.

Key Words: Sandwich, Syntactic foam, Paper Honeycomb core, Energy dissipation.

1. INTRODUCTION

Composite sandwich panel offer high strength, higher modulus and lower density. This is of utmost important in many applications such as aerospace, marine and automotive structures. Depending on whether the structural design is strength-critical or stiffness-critical, the material used should therefore have a high strength-to-weight ratio or a high stiffness-to-weight ratio.

Sandwich composites are produced by attaching two thin but stiff skins to a lightweight thick core. Some of the commonly used core materials are balsa, honeycomb, corrugated structures, polymeric foams and syntactic foams. The skins are normally made from FRP composites, metal sheets etc. Syntactic foam based sandwich composites are being used in various marine components and structures because of its versatile characteristics. Syntactic

foams (made by mixing hallow particles in resin matrix) have gained considerable importance as core materials in sandwich composites due to their high compressive strength, damage tolerance and low moisture absorption capability etc. The most important drawback of sandwich composite is their susceptibility to out of plane impact damage such as that imparted by the accidental fall of a tool. The problem associated with the nature of the impact damage, appears in the form of in-plane delaminations, matrix cracking, fiber matrix debonding, fiber shear-out and fiber fracture. The effects of impact damage on the mechanical properties of composites have been the subject of an intense investigation worldwide. In order to benefit from the prospective of these materials, better understanding of the impact response, damage tolerance and energy absorption capabilities is needed. An ideal structure requires that it uses stronger, stiffer, tougher and lighter material to absorb more energy under impact load. This is difficult to achieve using a single material because some of the requirements are obviously contradictory. It is suggested in most of that paper that hybridization in both materials and structures scales may be a way out. This may be a direction for developing high performance and impact tolerance composite structures.

Investigations made by Shih et.al [1] reveal that the impact response of composite sandwich panel was found to be mainly controlled by the face sheets and relatively independent of the density of PVC foam core, provided the face sheet material is tough enough. Vaidya et.al [2] found that the damage tolerance is enhanced by foam filled honeycomb core and impact load required to initiate the damage is independent of the face sheets. Anderson et.al [3] carried out experimental investigation to characterize the type and extent of the damage observed in a variety of sandwich configurations with graphite/epoxy face sheets using foam and honeycomb cores. They concluded that, as the impact energy was increased, the samples experienced one of two types of damages: a tear or crack from the center of the laminate to the edge, or significant damage consisting of a dent localized in the region of impact. Liaw et.al [4] investigated impact-induced delamination and fracture in 6061-T6 aluminum/cast acrylic sandwich plates adhered by epoxy were generated in an instrumented drop-weight impact machine. The impact tests were conducted at various temperatures. Results of their investigation reveal that the temperature has a significant influence on impact damage. Vaidya et.al [5] focused on impact damage of partially foam-filled co-injected honeycomb core sandwich composites. They concluded that low cost phenolic impregnated kraft paper core in conjunction with polyurethane or syntactic foam offers significant cost-savings over traditional cores such as nomex or PMMA foams and offers superior impact performance. Hosur et.al [6] detailed about the manufacturing and low-velocity impact characterization of hollow integrated core sandwich composites with hybrid face sheets. Results of their study indicate that the provision of additional face sheets considerably enhances the damage resistance. Jiang et al [7] discussed about the local displacement of core in two-layer sandwich composite structures subjected to low velocity impact. Results reveal that two-layer sandwich panels promise to reduce the local displacement of the core significantly.

Meo et.al [8] experimentally determined low-velocity impact response of composite sandwich structure of the engine nacelle fan cowl doors of a large commercial aircraft at energy levels ranging from 5 to 20 J. Results from the impact-damage C-scan test indicate that significant internal damage occurs at relatively low impact-energy levels, which can significantly reduce the residual strength of the panel. Low velocity impact, compression after impact, and tensile stiffness properties of carbon fiber and Kevlar fiber combination sandwich composites were investigated by Jeremy Gustin et.al [9] in their study. They found that, for the entire set of samples tested, partial/total face sheet penetration occurred for the 5–10 J impacts, total face sheet and partial core penetration for the 15 J impacts, and partial/total bottom face sheet penetration for the 20–45 J impacts. Hosur et.al [10] fabricated sandwich panels with neat and nano-phased foam cores and three layered plain weave carbon fabric/epoxy-nano clay composite face sheets. They conducted impact test and found that samples with nano-sized foam sustained higher impact load and had lower damage area as compared with neat

counter parts. Berketis et.al [11] discussed about the influence of long term water immersion ageing on impact damage behavior and residual compression strength of glass fiber reinforced polymer. Immersion ageing was followed by low velocity impact tests and post impact compression test. Results from compression after impact (CAI) test shows reduction in CAI strength, due to hydrothermal exposure for each applied level of impact forcing. Low-velocity impact failure of aluminum honeycomb sandwich panels discussed by Foo et.al [12] concluded that denser cores exhibited greater peak impact loads and experienced smaller damage profiles in the core and impacted face sheet. Flores-Johnson et.al [13] investigated the effects of the impactor nose shape on the penetration behavior of polymethacrylimide (PMI) foams is investigated in the velocity range of 4-8 m/s. It is observed from experimental results that penetration impact load depends on the geometry of the impactor and the density of the foam.

The main intuition behind the present investigation is to improve the energy absorption characteristics of syntactic foam-cored sandwich composites under out-of-plane impact loading conditions. In the present work, the concept of foam filled honeycomb construction was applied to develop RIPH infused syntactic foam cores. Further, syntactic foam infused with RIPH structure was additionally strengthened by providing face-sheets. E-glass/epoxy laminates were used as materials for face sheet. Sandwich composites typically used in ship hull construction will be subjected to out-of-plane low velocity impact loads. Hence, sandwich composite coupons tested for impact and energy absorption properties using low-velocity impact test configurations to determine the viability of using the same for marine structural applications.

2 MATERIALS AND METHODS

2.1 RAW MATERIALS

Sandwich composites examined in the present work were virtually identical in every respect such as type of glass fabric, resin systems, grades of Cenosphere and their composition. Three types of cores made from the blend of Cenosphere (hallow particles) and phenolic resin with 0.5 mass fraction of Cenosphere. Cenosphere extracted from fly ash – a waste material from thermal power plants supplied by Cenosphere India Ltd, Kolkata. Cores were developed using warm press molding technique at a temperature of 140-150 ^{0}C for 15 minutes. The main difference between three types of core was the type of RIPH structure infused in it. The RIPH structure (**Fig. 1**) developed from Nomex® paper (EI Dupont India Pvt., Ltd., Bombay) and recycled Kraft paper (Vasper Green Technologies, Bangalore) by screen printing technique followed by phenolic resin impregnation and then cured at 150 ^{0}C. Nomex based RIPH structure infused syntactic foam is named as SFNC and kraft based RIPH structure infused syntactic foam is named as SFKC. However, syntactic foam without RIPH structure is named as SFC. Cores (**Fig. 2 a**) were additionally strengthened by E-glass/epoxy laminates (**Fig. 2 b**) (face sheets) with 0.65 fiber volume fraction using wet lay-up followed by vacuum bonding technique. The fabric had an average filament diameter of 12microns and an areal weight of 0.185 kg/m^2. Table 1 details the developed sandwich composites with three types of cores.

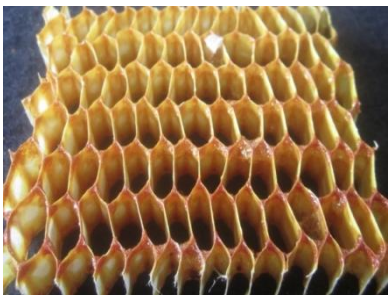

(a) **(b)**

Fig. 1 (a) Phenolic resin impregnated Kraft paper honeycomb core

(b) Phenolic resin impregnated Nomex paper honeycomb core

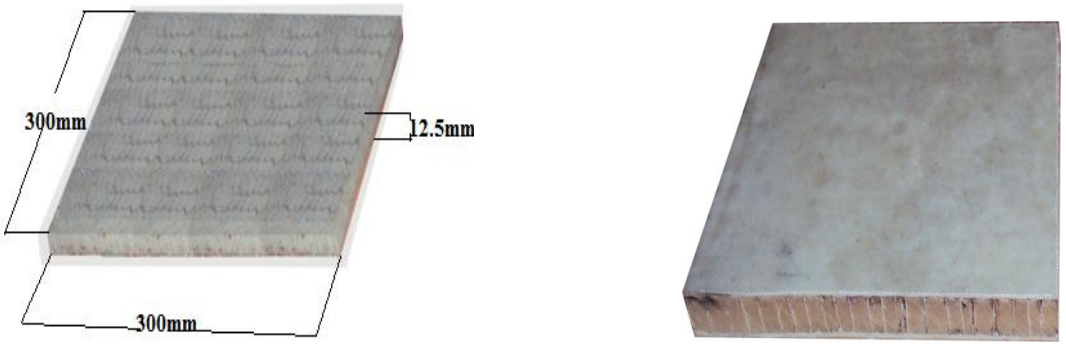

(a)

(b)

Fig. 2 **(a)** Syntactic foam infused with RIPH Core structure
(b) Sandwich composites with core of syntactic foam infused with RIPH structure

Table 1. Details of the sandwich composites

Sandwich designation	Core material	Face sheet Material
S1	Nomex Honeycomb (NC)	E-glass/epoxy
S2	Kraft Honeycomb (KC)	E-glass/epoxy
S3	Syntactic Foam (SFC)	E-glass/epoxy
S4	Syntactic Foam filled Nomex Honeycomb (SFNC)	E-glass/epoxy
S5	Syntactic Foam filled Kraft Honeycomb (SFKC)	E-glass/epoxy

2.2 Low velocity Impact Test

It was found that, the energy absorption capability in terms of toughness of the developed sandwich composites S3, S4and S5 were found to be much higher compared to S1 and S2 sandwich composite coupons. Hence, sandwich composites S3, S4, and S5 were subjected to low-velocity impact test using Instron dynatup 8250 drop weight Impact testing machine. The machine consists of an instrumented drop-weight hemispherical tup of 0.3 kg and 10 mm diameter (load cell), velocity detector and GRC 730-I data acquisition system that records the impact events such as load, energy, deflection and velocity as a function of time. A latching mechanism present in the machine prevents multiple impacts. The mass and drop height of the impactor can be varied to accommodate wide range of energy levels.

The initiation and propagation energy were determined using these data. Impact energy corresponding to the maximum impact load is defined as initiation energy. Propagation energy is defined as the difference between the maximum impact energy and the initiation energy. Also, a dimensionless parameter called the ductility index (DI), was evaluated which is found useful for ranking the impact performance of different sandwich composite under similar testing conditions. The DI is defined as the ratio between the propagation energy and the initiation energy [14]. The sandwich composite coupons (**Fig. 3**) of size 150 mm × 150

mm × 15.5 mm were clamped on all the four sides in the supporting fixture and tested at energy levels of 45 J and 60 J so as to obtain clearly visible dents on the coupons. For each type of sandwich composite, three identical coupons were tested and average results are reported.

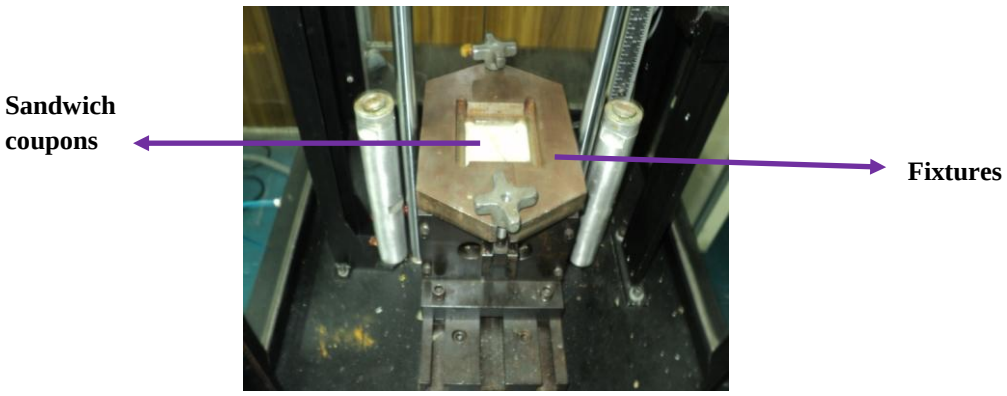

Fig 3 Configuration of Sandwich composites in fixture of Instron dynatup 8250 machine

3 RESULTS AND DISCUSSION

In the event of low velocity impact of sandwich composites S3, S4, and S5 have shown that the disturbance is transferred from the point of impact in the form of longitudinal waves and transverse waves in outward direction. Meanwhile, energy dissipation takes place in the form of energy transfer and energy absorption mechanisms. The mechanism of energy absorption in all sandwich composites takes place primarily through indentation (plastic deformation), delaminating, matrix cracking, fiber fracture and fiber/matrix interfacial debonding at the E-glass/epoxy laminated face sheets. In addition to this, cores (SFC, SFNC and SFKC) serve to absorb energy through densification, matrix cracking, and Cenosphere crushing and interfacial debonding. Regardless of the particular mechanisms, it is concluded that the energy is absorbed through damage and permanent deformation.

Fig. 4 and Fig. 5 shows the load-time-energy plots of S3, S4 and S5 sandwich composites at the impact energy levels of 45J and 60J respectively. Impact load increases with the increase in impact energy levels. The magnitude of peak load indicates the impact strength of the materials. Higher the peak load, higher will be the impact strength indicating the ability of the material to resist the higher impact loads (**Fig 4-5**). The impact load-time curves of all the sandwich composite coupons have into two distinct phases; damage initiation and damage propagation. The damage initiation phase starts from zero to the first peak of the impact load. The damage propagation phase starts at the end of the damage initiation phase to the point where the impact load drops back to zero. The damage initiation phase clearly indicates the mechanism of energy transfer in terms of initiation energy, while damage propagation phase indicates the mechanism of energy absorption in terms of propagation energy.

It can be seen that, the impact load carrying capability of all types of sandwich composites are almost same. The sudden drop in the load-time plot of S3 coupon is an indication of their brittle nature, whereas, S4 and S5 indicated ductile behavior as can be seen by gradual rise and drop in the load-time plots. Further, an energy dissipation characteristic of sandwich composites (S4 and S5) is considerably improved by the infusion of RIPH structure in syntactic foam core (**Table 2**). Initiation energy of S4 and S5 sandwich coupons is found to

be higher as compared with S3 coupons, which in turn indicates their greater resistance to the initiation of crack. The presence of RIPH structure in syntactic foam makes the composite stiff and strong. Also, S4 and S5 sandwich coupons exhibit significantly higher propagation energy than S3 coupons, indicating greater resistance to the propagation of crack. Generally, lower initiation energy and higher propagation energy in all sandwich coupons, leads to higher value of ductility index (DI). Moreover, higher value of ductility index (>1) indicates that the energy dissipation is mainly through damage propagation [14]. Thus, once the damage is initiated, there is wide spread propagation of the cracks in transverse direction. Similar behavior was observed by Guoqiang Li et.al [15-16] in their work with glass micro balloon-epoxy based syntactic foam. It can be seen that, in S4 and S5 sandwich coupons with the core of RIPH structure in syntactic foam, the resistance to damage initiation has improved and more energy has been absorbed through damage propagation. The syntactic foam and RIPH with hexagonal cells structure provide synergistic support to each other. The RIPH structure prevents the syntactic foam from crushing under transverse load, while the syntactic foam provides constraints for the RIPH structure from lateral deformation under transverse loads. This is very interesting from the point of energy transfer and energy absorption capabilities of the sandwich composites.

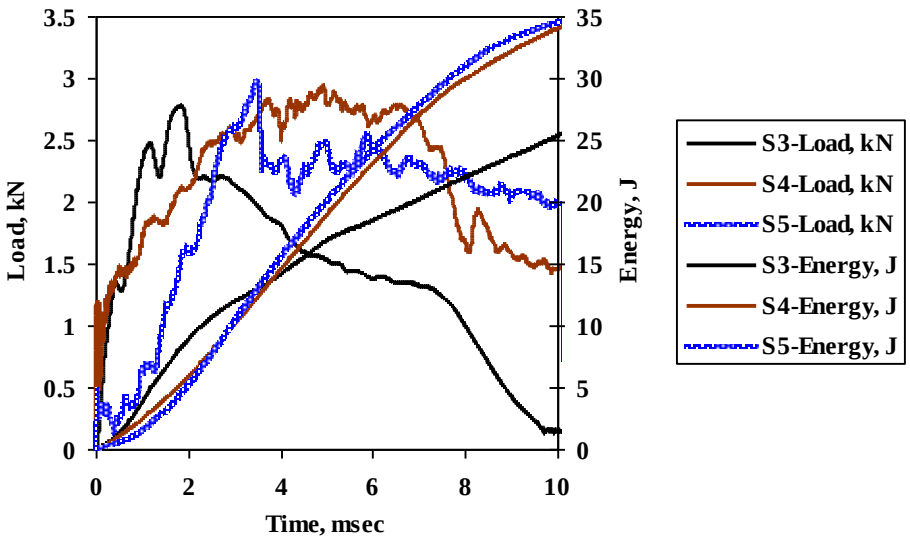

Fig. 4 Impact load-energy-time plot of three types of sandwich composites at 45J

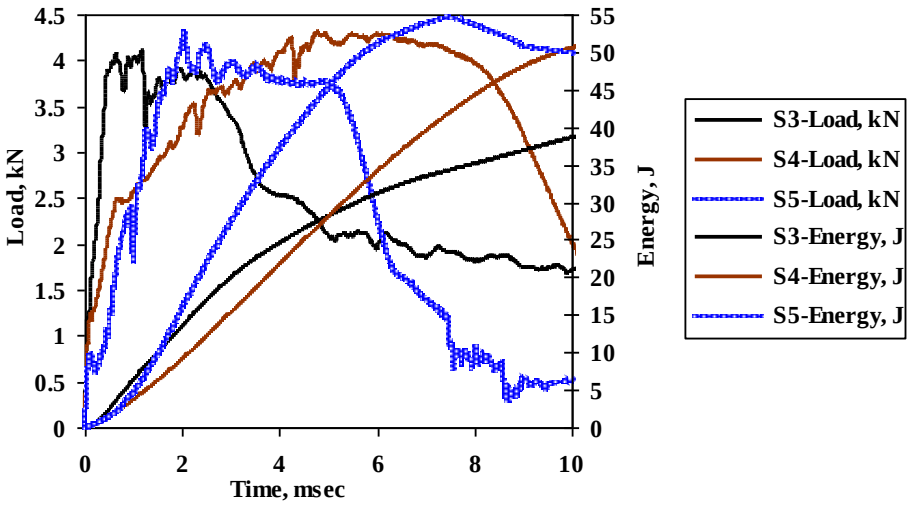

Fig. 5 Impact load-energy-time plot of three types of sandwich composites at 60 J

Table 2. Impact test results with energy levels of 45J and 60J

Energy Level (Joule)	Sandwich Coupons	Peak Impact load (kN)	Initiation Energy (Joule)	Propagation Energy (Joule)	Energy Absorption (Joule)	Ductility Index (DI)
45	S3	2.71	9.49	15.88	25.37	1.67
	S4	2.87	14.27	20.28	34.55	1.42
	S5	2.93	13.62	20.86	34.48	1.53
60	S3	4.09	12.08	26.58	38.66	2.20
	S4	4.28	19.73	30.59	50.32	1.55
	S5	4.26	19.25	30.62	49.87	1.59

4 CONCLUSION

An attempt has been made to improve the energy absorption characteristics of syntactic foam-cored sandwich composites. This is done by the infusion of RIPH structure in syntactic foam core during manufacturing. The developed sandwich composites (S3, S4 and S5) were subjected to low-velocity impact test at 45J and 60J energy levels. Based on the investigation, following conclusions may be drawn.

- Syntactic foams can effectively dissipate the impact energy in the form of both energy transfer (in terms of initiation energy) and energy absorption (in terms of propagation energy).
- It is found that syntactic foam that is having high propagation energy, suggesting that it is the best composition in terms of energy absorption.
- The mechanism of energy absorption in all sandwich composites takes place primarily through indentation (plastic deformation), delamination, matrix cracking, fiber fracture and fiber/matrix interfacial debonding at the E-glass/epoxy laminated face sheets. In addition to this, cores (SFC, SFNC and SFKC) serves to absorb energy through densification, matrix cracking, cenosphere crushing, interfacial

debonding and transverse cracking within core followed by intact/delamination of the bottom face sheets. The extent of delamination was much higher on the tensile side.

- Comparing S4 and S5 with S3sandwich composites, it is found that the initiation and propagation energy of the S4 and S5 sandwich coupons is higher. This suggests that the infusion of RIPH structure in syntactic foam core serves to increase energy transfer and energy absorption characteristics.
- Higher value of ductility index (>1) indicates that the energy dissipation is mainly through damage propagation leads to higher energy absorption capability of sandwich structures.
- S4 and S5 sandwich composites have shown impact behavior in ductile manner with higher initiation and propagation energy as compared with S3 coupons. Higher initiation energy suggests their high stiffness and strength, while higher propagation energy suggests their high toughness.
- Finally it can be concluded that improved energy dissipation characteristics of the RIPH structure infused syntactic foam core sandwich composite promises its applications in stiffness critical marine structures.

REFERENCES

[1] Shih W K, Jang B Z. Instrumented Impact Testing of Composite Sandwich Panels, Journal of Reinforced Plastics and Composites1989; 8(3): 270-298.

[2] Vaidya U K, Kamath M V, Mahfuz H & Jeelani S. Low Velocity Impact Response of Resin Infusion Molded Foam Filled Honeycomb Sandwich Composites, Journal of Reinloaded Plastics and Composites1998;17(9): 819-849.

[3] Anderson T, Madenci E. Experimental investigation of low-velocity impact characteristics of sandwich composites. Composite Structures 2000; 50: 239-247.

[4] Liaw B M, Zeichner G, Liu Y X. Impact Delamination and Fracture in Aluminum/Acrylic Sandwich Plates. Proceedings of the SEM IX International Congress on Experimental Mechanics June 5-8, 2000, Orlando, Florida.

[5] Vaidya U K, Ulven C, Pillay S,Ricks H. Impact Damage of Partially Foam-filled Co-injected Honeycomb Core Sandwich Composites. Journal of composite materials 2003; 37(7):611-626.

[6] Hosur M V , Abdullah M, Jeelani S. Manufacturing and low-velocity impact characterization of hollow integrated core sandwich composites with hybrid face sheets. Journal of Composite Structures 2004; 65: 103-115.

[7] Dazhi Jiang, Dongwei Shu. Local displacement of core in two-layer sandwich composite structures subjected to low velocity impact. Journal of composite structures 2005; 71: 53-60.

[8] Meo M , Vignjevic R, Marengo G. The response of honeycomb sandwich panels under low-velocity impact loading. International Journal of Mechanical Sciences 2005; 47 : 1301–1325.

[9] Jeremy Gustin, Aaran Joneson, Mohammad Mahinfalah, James Stone. Low velocity impact of combination Kevlar/carbon fiber sandwich composites. Composite Structures 2005; 69: 396–406.

[10] Hosur M V, Mohammed A A, S. Jeelani. Processing of Nanoclay Filled Sandwich Composites and their Response to Impact Impact loading. Journal of Reinloadd Plastics and Composites, Vol. 27, No. 8, 797-818 (2008).

[11] Berketis K, Tzetzis D, Hogg P J. The influence of long term water immersion ageing on impact damage behavior and residual compression strength of glass fibre reinloadd polymer. Journal of Materials & Design 2008; 29:1300-1310.

[12] Foo C C, Seah L K, Chai G B, Low-velocity impact failure of aluminium honeycomb sandwich panels. Composite Structures 2008; 85: 20–28.

[13] Flores Johnson E A, Li Q M. Low Velocity Impact on Polymeric Foams. Journal of Cellular Plastics 2011; 47(1): 45-63.

[14] Pegoretti, A., Cristelli, I., Migliaresi, C., Experimental optimization of the impact energy absorption of epoxy-carbon laminates through controlled delamination, Composites Science and Technology (2008), doi: 10.1016/j.compscitech.2008.04.036

[15] Guoqiang Li, Nji Jones. Development of rubberized syntactic foam. Composite Part A: Applied Science and Manufacturing 2007;38(6):1483-1492

[16] Guoqiang Li, Jinquan Cheng, Su-Seng Pang. Experimental study of composite sandwich structures with a grid stiffened hybrid core. 14th international conference on composite/nano composite engineering, Boulder, Colorado, July 2-8, 2006.

Proceedings of 7th National Conference on Multidisciplinary Research in Science & Engineering, MIT AOE Alandi, Pune, 3-4 June 2016 ,pp. 9-16, ISBN: 978-93-84659-59-2

OPTIMIZATION OF FADING FUNCTIONS IN TEMPORAL SPLITTING FOR BINAURAL DICHOTIC PRESENTATION

Zeba Bhaktiyar Mangalore and P.N.Kulkarni
Department of ECE, Basaveshwar Engineering College, Bagalkot, India

Abstract

In this paper, an optimal shape of fading functions for temporal splitting of speech signal is found for binaural dichotic presentation. The purpose of temporal splitting is to overcome the adverse effects of temporal masking in sensorineural hearing loss. The fading functions used in proposed work are step transition, trapezoidal and half cosine function. The binaural dichotic presentation is a method to reduce the effect of masking, and this can be accomplished by utilizing the complementary fading functions for processing the speech signal. The test signals used are sinusoidal and chirp signal. The spectrograms obtained for the temporally split signal presented to two ears, are analyzed for spectral leakage in PRAAT software. On the basis, objective assessment of spectral distortion using spectrograms, obtained after processing test signal with the different fading functions, the optimal fading function was selected for binaural dichotic presentation.

Key Words: Binaural dichotic presentation, Temporal masking, Half cosine function.

1 INTRODUCTION

Sensorineural hearing loss is characterized by temporal and spectral masking. Masking is a phenomenon in which the perception of a signal is reduced because of the presence of the masking signal. The effect of spectral masking and temporal masking on speech perception can be reduced using the method of binaural dichotic presentation [1]. Binaural dichotic presentation involves splitting of speech signal using two different fading functions, complementary to each other. The step transition and trapezoidal fading function with interaural switching period of 20ms was implemented to decrease the effect of temporal masking. The effect of different slope transition and different duty cycle had been studied [2][3]. Effects of different types of fading functions and overlap (duty cycle greater than 50%) in reducing the perception of temporal gaps due to switching and in improving speech intelligibility was studied. The splitting of speech signal into the two channels can be carried out in a number of ways. The signal is split in two signals with complementary spectra using critical band of filters to reduce the spectral masking. This approach leads to improved reception of consonants [4][6][7].

The shape of temporal windows plays an important role in reducing the effect of temporal masking. Among the exponential, Hann and rectangular windows, a study on optimal shape was undertaken using Computational Auditory Signal-processing and Perception (CASP) model. CASP model was used to calculate the root mean square error (RMSE) value of target audio signal and another interfering audio signal. Effect of step, shape and overlap of these windows was studied. Shorter steps and greater overlap of all the windows resulted into low RMSE, indicating robustness of the model [5].

The aim of this paper is to study the effect of different fading functions on testing signals. The fading functions are step transition function, trapezoidal and half cosine function. The test signals included are sinusoidal and chirp signal. The spectrograms of the temporally split test signals are analyzed on the basis of spectral leakage, so as to select the best fading function among the three.

In section II, the proposed method is described briefly, section III describes the implementation method; section IV includes results and section V concludes the future scope of the proposed work.

2 PROPOSED WORK

In binaural dichotic presentation different signals are presented to left and right ear. Figure 1 shows the schematic block diagram of binaural dichotic presentation. S(n) is the speech signal, that is temporally split using fading functions $f_1(n)$ and $f_2(n)$ resulting into $S_1(n)$ and $S_2(n)$ respectively. The fading functions $f_1(n)$ and $f_2(n)$ are complementary to each other, on time scale as shown in figure 2, where the fading functions considered have a step transition. If N is the time period and L is the ON-period of the step function then duty cycle is defined by equation d=L/N, and $f_1(n)$ and $f_2(n)$ can be defined as

f1(n)=1, $0 \leq n \leq L-1$
=0, otherwise
f2(n)=0, $L-N/2+1 \leq n \leq N/2$
=1, otherwise

If N samples signal is multiplied with fading functions with duty cycle of 50%, after temporally splitting, N/2 samples are presented to left ear relaxing right ear and alternately next N/2 samples to right ear relaxing left ear. Perceptually both left and right ear information gets integrated into common information at the higher level in the brain. This results in reducing the effect of temporal masking. $S_1(n)$ and $S_2(n)$ are temporally split signals presented to left and right ear respectively. The spectrograms of $S_1(n)$ and $S_2(n)$ signals are analyzed based on spectral leakage, to select the appropriate shape of fading function for temporally splitting of speech signal in binaural dichotic presentation.

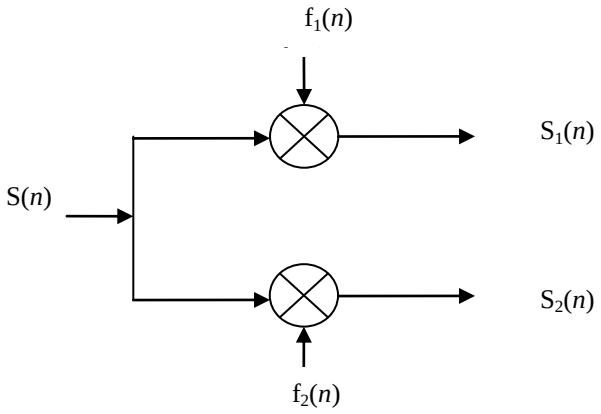

Figure 1: Binaural dichotic presentation

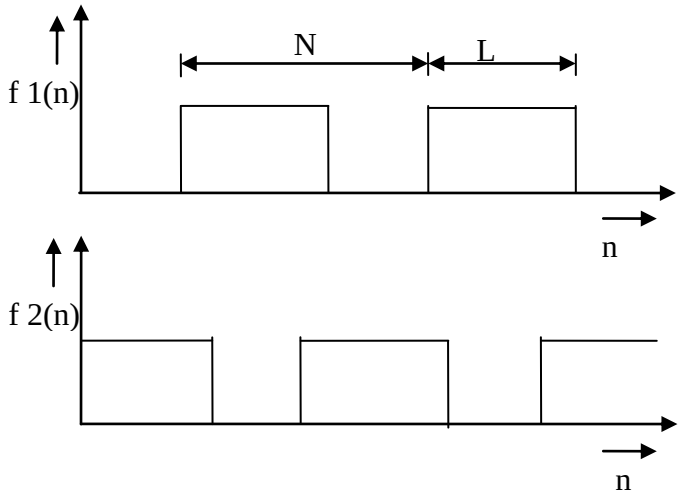

Figure 2: Step transition fading function

3 IMPLEMENTATION

The three fading functions that are implemented in this proposed work are step, trapezoidal and half cosine signal. The fading functions frequency is 4 Hz and sampled at 16000 samples per second. The test signals are sinusoidal signal of frequency 1000 Hz and a chirp signal with linear variation of 500 to 5000 Hz. The sampling frequency of test signal is 16 KHz. The test signals and fading functions is generated using MATLAB tool. Figure 3, Figure 4 and Figure 5 shows the step, trapezoidal and half cosine signals respectively that are implemented in proposed work. From figures it is clearly evident that the processed test signal are presented alternately to the two ears. Testing signal is processed with each fading function to present dichotically to two ears.

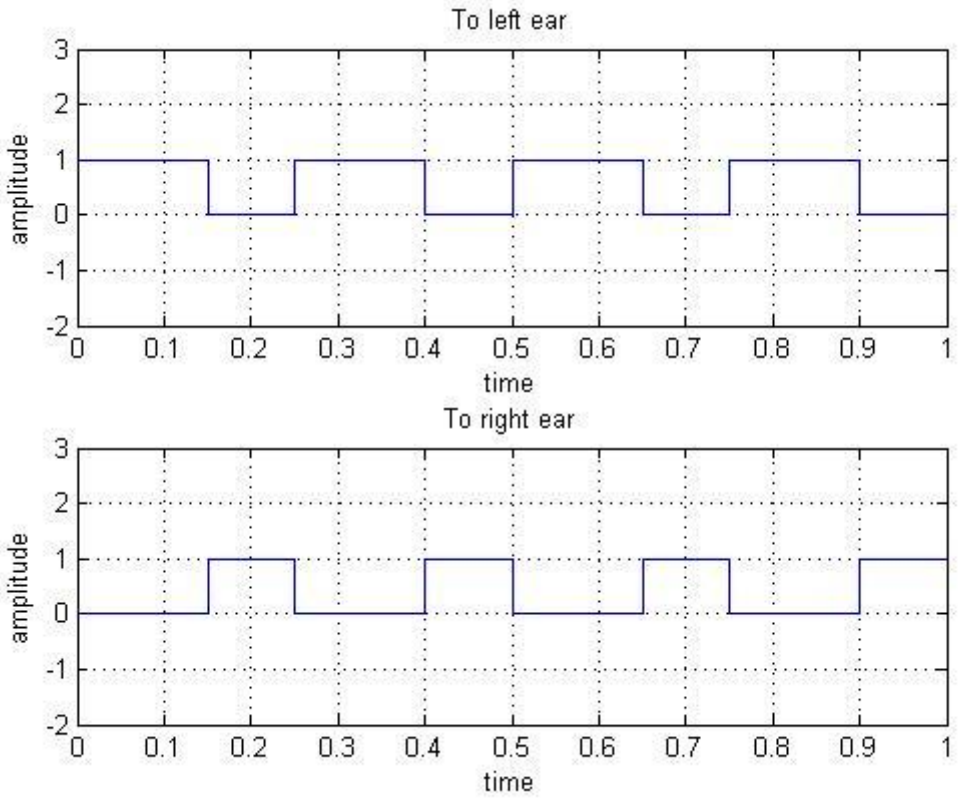

Figure 3: Step transition fading function

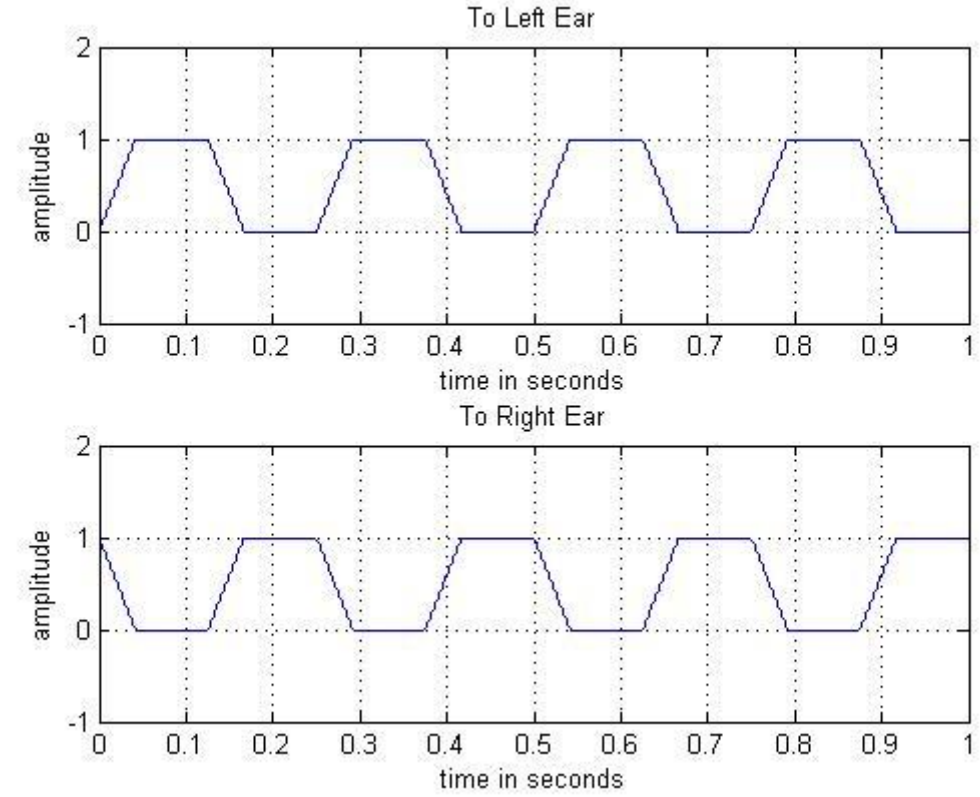

Figure 3: Trapezoidal fading function

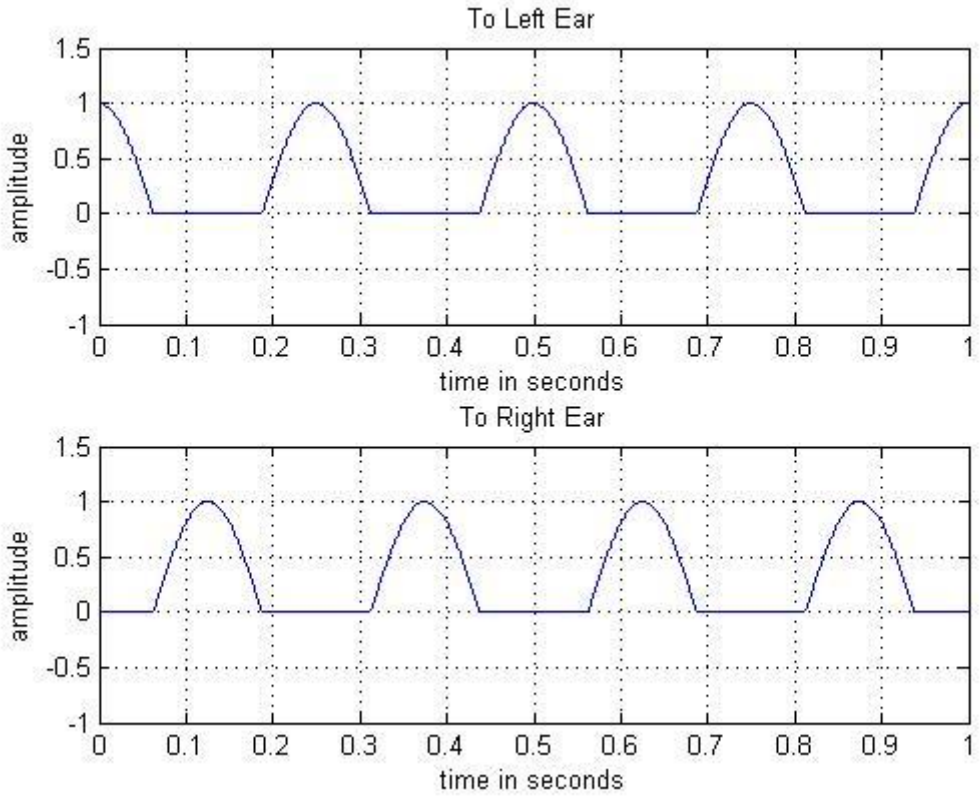

Figure 4: Half cosine function

The spectrograms of the temporally split test signal are analyzed using PRAAT software.

4 RESULTS

The temporally splitting of chirp signal using step transition and half cosine fading function is analyzed using MATLAB as shown in Figure 6 and Figure 7.

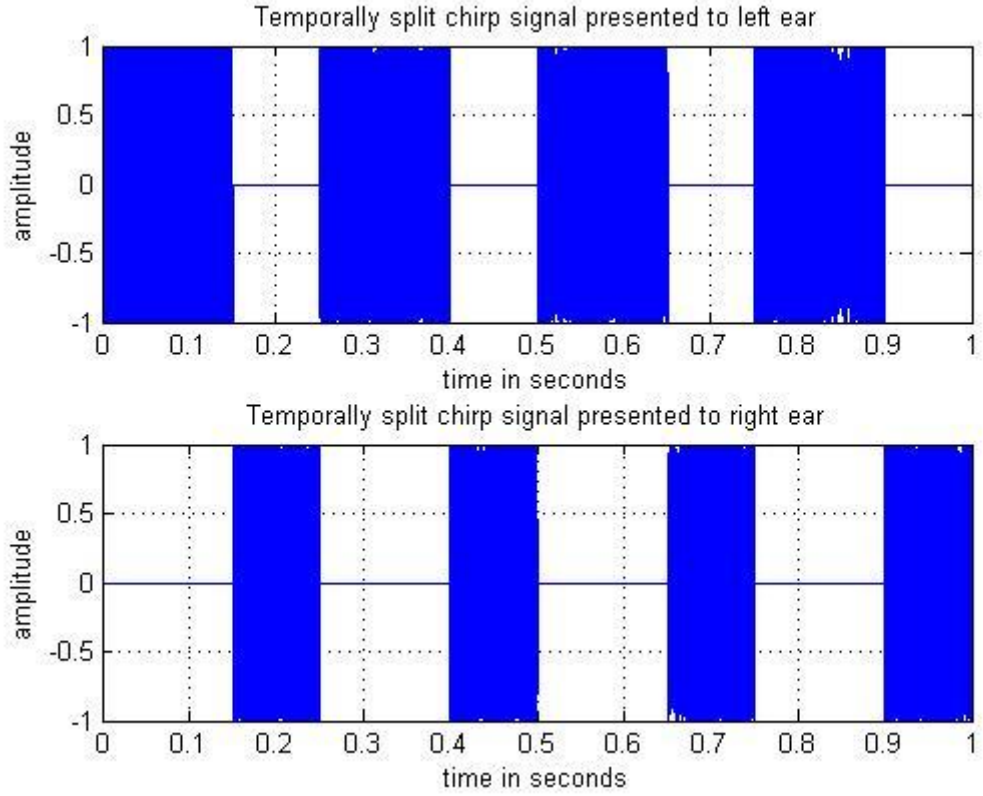

Figure 6: Temporal splitting of chirp signal using step function

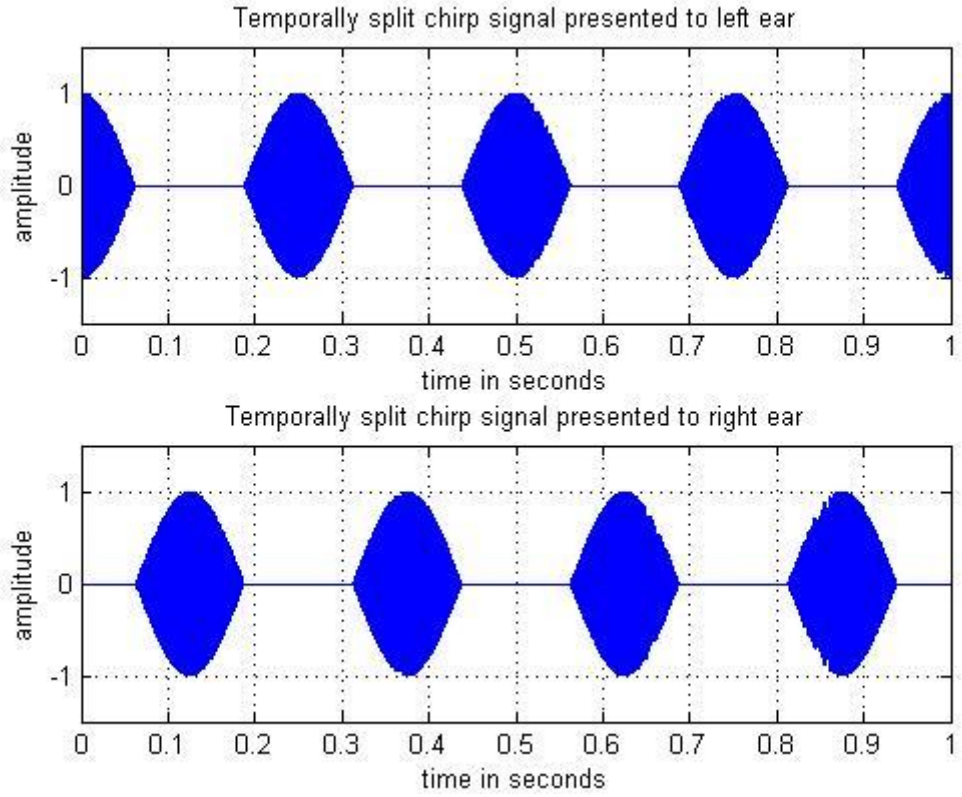

Figure 7: Temporal splitting of chirp signal using half cosine function

The spectrogram of the chirp signal linearly varying from 500 Hz to 5000 Hz is as shown in Figure 8. The spectrogram of the temporally split chirp signal using step transition is analyzed in PRAAT software as shown in Figure 9. The sharp edges at the transition of fading functions introduce the spectral leakage and hence spectral distortion. This leads to poor signal quality of processed signal. Spectral leakage is due to localized spreading of frequency components and it depends on shape of fading functions. Figure 9.a and 9.b shows the spectrogram of temporally split chirp signal using step transition fading function, presented to left and right ear respectively. The spectral leakage is less when trapezoidal fading function is used but it is considered to be more when compared to half cosine function.

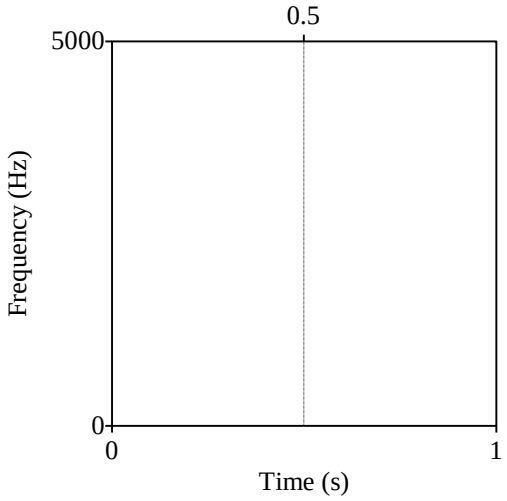

Figure 8: Spectrogram of chirp signal linearly varying from 500 Hz to 5000 Hz

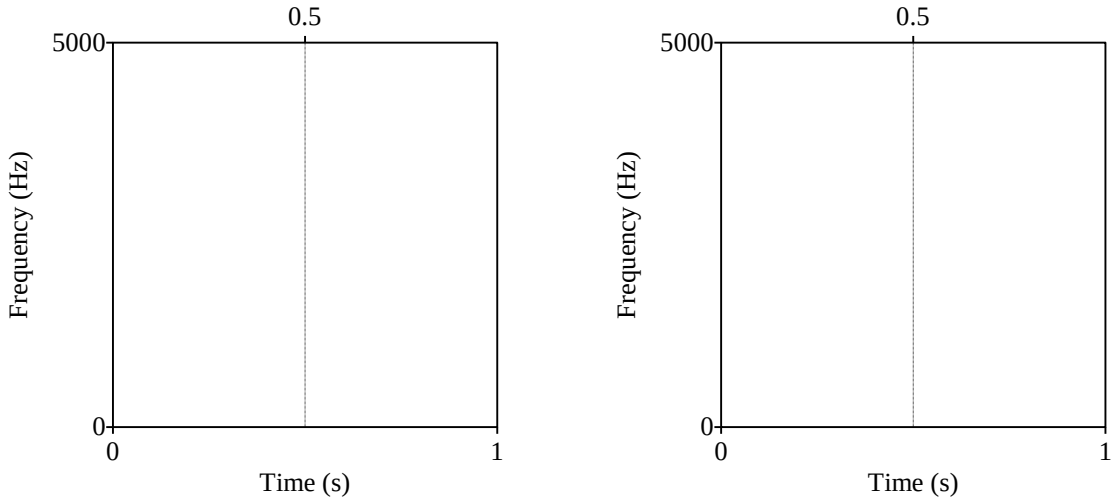

(a) Left ear (b) **Right ear**

Figure 9: Spectrogram of the temporally split chirp signal using step transition fading function and presented to left and right ear

Figure 10 shows the spectrogram obtained when chirp signal varying from 500 Hz to 5000 Hz, is processed using half cosine function. The spectral leakage is less as compared to the spectral leakage in other fading functions considered. Figure 10.a and 10.b shows the spectrogram of temporally split chirp signal using half cosine fading function, presented to left and right ear respectively.

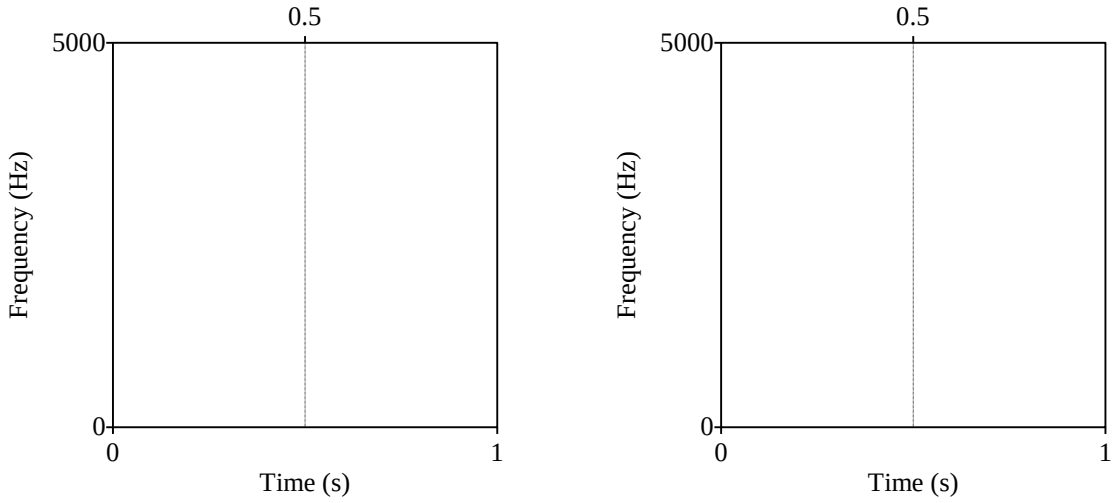

(a) Left ear (b) **Right ear**

Figure 10: Spectrogram of the temporally split chirp signal using half cosine function and presented to left and right ear

Same analysis and results are carried and obtained for sinusoidal test signal.

5 CONCLUSION

The results proved that the shape of fading function provides an impact on deteriorating the speech or signal quality. Based on the results of spectrograms obtained, the half cosine function resulted into less spectral leakage as compared to step and trapezoidal fading function. Therefore half cosine function is selected as better fading function in binaural dichotic presentation. The exact complementary fading functions results into lateralization and perceptual imbalance in loudness of perceived speech. Hence to avoid it the half cosine signal with an appropriate overlap

has to be generated and its effect on improvement of speech quality and intelligibility has to be studied.

REFERENCES

[1] Pandurangarao N. Kulkarni, Prem C. Pandey and Dakshayani S. Jangamashetti, “Binaural dichotic presentation to reduce the effects of spectral masking in moderate bilateral sensorineural hearing loss”, International J. Audiology, Vol.51, 2012, pp.334-344.

[2] D. S. Jangamashetti and P. C. Pandey, “Dichotic presentation with inter-aural switching for reducing the effect of temporal masking due to sensorineural hearing loss”, in Proc. National Conference on Biomedical Engg., Roorkee, India., April 2000, pp. 346-353.

[3] D. S. Jangamashetti and P. C. Pandey, “Inter-aural switching with different fading functions for dichotic presentation to reduce the effect of temporal masking in sensorineural hearing loss”, in Proc. 4th World Multi Conference on Systemics, Cybernetics and Informatics (SCI'2000), Orlando, Fl. USA, pp.346-353.

[4] D. S. Chaudhari and P. C. Pandey, “Dichotic presentation of speech signal with critical band filtering for improving speech perception,” Proc. ICASSP’98, Seattle, Wash., U.S.A., pp.3601-3604.

[5] Khan Baykaner and Soren Bech, “Selection of temporal windows for the computational prediction of masking thresholds”, in Proc. ICASSP, 2013, pp. 408-412.

[6] Alice N.Cheeran and Prem C. Pandey, “Speech processing for hearing aids for moderate bilateral sensorineural hearing loss,” in Proc. ICASSP, 2014, pp. 1V-17 -20.

[7] Alice N. Cheeran and Prem C. Pandey, “Evaluation of speech processing schemes using binaural dichotic presentation to reduce the effect of masking in hearing-impaired listeners,” in Proc. 18th International Congress on Acoustics, ICA 2004, Kyoto, Japan, pp. II-1523 -1526.

Proceedings of 7th National Conference on Multidisciplinary Research in Science & Engineering, MIT AOE Alandi, Pune, 3-4 June 2016, pp. 17-24, ISBN: 978-93-84659-59-2

INFERENTIAL ANALYSIS BASED ON CHI-SQUARE TEST FOR INDEPENDENCE OF ATTRIBUTES UNDER STUDY

K.S. Borase[1] and S.M. Khairnar[2]

[1]Assistant Professor in Mathematics, Department of Mathematics, RNC Arts, JDB Commerce and NSC Science College, Nasik Road (M.S.)

[2]Professor & Head, Department of Engineering Sciences, Dean (R & D), MIT AOE, Alandi, Pune

Abstract

The χ^2 test applies only to discrete data, counted rather than measured values. It is a test of independence, the idea that one variable is not affected by, or related to, another variable. The χ^2 is not a measure of the degree of relationship. It is merely used to estimate the likelihood that some factor other than chance (sampling error) accounts for the apparent relationship.

Statistical inferences are not made with certainty but are based upon probability estimates. These are indispensible tool in research that enables it to make generalizations about populations from their observations of the characteristics of samples[7].

Key Words: The Chi-square test, attributes, Likert's Scale limits of functions and graphs.

1. INTRODUCTION

Together with philosophy, Mathematics is the oldest academic discipline known to mankind[3]. Today mathematics is a huge complex enterprise, far beyond the keen of anyone individual. Those of us who choose to study the subject can only choose a piece of it, and in the end, must specialize rather drastically in order to make any contribution to the evolution of ideas.

This research article provides an outline of the current research in students' understanding of topics in limits of function by using graphs rather than traditional method of teaching[2]. The sample size of data under study is 500 (250 boys and 250 girls) of the population 5000. The deliberately lectures has been arranged for the Experimental and Controlled groups of size 250 each. The questionnaire and interviews has been carried out the results thus obtained has been analyzed. The intent of work is to provide an overview of specific difficulties based on education research in the subject communication in Mathematics in the context of limits of functions by the students mainly accepted the assumptions based on literacy, confidence and curiosity along with the living status and gender differences among the students[6].

The following tools have been used to record the observations:

- Measurement of Curiosity Level of the Students:

Options		Rating
Fully Solved	:	2
Partially Solved	:	1
Not solved	:	0

- Confidence Level Scale:
  By using Dr.Rensis Likert's Scale Technique:
  "The teaching-learning model/aid IOA is helpful in teaching-learning process of theory of limits". (Hypothesis/Assumption)
  1: Strongly Agree, 2: Agree, 3: Neither, 4: Disagree & 5: Strongly Disagree.
- Family Members Literacy Scale:
  0: None (Mother or father or guardian) is educated,
  1: Either (Mother or Father or Solo guardian) is educated,
  2: Both (Mother, Father or Guardian parents) are educated.
- Residential Status of the Students:
  R: Rural, U: Urban

2. RELATION BETWEEN LITERACY AND LIVING STATUS OF STUDENTS TOWARDS UNDERSTANDING OF LIMIT CONCEPTS

In this case, respondents (students) were asked their views concerning whether it is an effectible of literacy of their parents along with their residence location to understand the concept of limits of functions[5].
The hypotheses have been made to check whether or not the literacy of family members of the students and their living status are associated. For this the null and alternative hypotheses were as under:
H_0: No relation between literacy and living location for understanding of mathematical concept of limits.
H_1: Some relation between literacy and living location for understanding of mathematical concept of limits.
Rejection or acceptance of the hypothesis is based on the Chi Square test.
Table 2.1 gives a cross classification of respondent's literacy of family members by respondent's opinion concerning of understanding of limit concept. Notice that three point literacy scales has been used with the categories being none (mother or father or guardian) is educated, either (mother or father or solo guardian) is educated and both (mother, father or guardian parents) are educated.

TABLE 2.1
Association between Literacy and Living Status towards Understanding of Limit Concept

Living Status	**Literacy of Family Members of Students**			**Row Total**
	None	**Either**	**Both**	
Rural	15	118	88	**221**
Urban	18	167	104	**279**
Column Total	**23**	**285**	**192**	**500**

Chi-Square	**Value**	**DF**	**Significance**
Pearson	6.293	2	0.043

The χ^2 table value for 0.05 significance and 2 degrees of freedom gives a critical value of 5.992. At 0.05 significance, the region of rejection of H_0 is all Chi square values of 5.992 or more.

Since 6.293 > 5.991, the Chi square value from the table is in the region of rejection of the null hypothesis and the null hypothesis of no relationship between literacy of family members and living status of students can be rejected. The small *p*-value (=0.043) strongly supports rejection of H_0.

Therefore at the 0.05 level of significance, there is evidence of a relationship between literacy of family members and living status of students while learning limit concepts.

3. RELATION BETWEEN CONFIDENCE AND LIVING STATUS OF STUDENTS TOWARD UNDERSTANDING OF LIMIT CONCEPTS

In this case, respondents (students) were asked their views concerning whether it is an effectible of confidence level along with their residence location to understand the concept of limits of functions.

The hypotheses have been made to check whether or not the confidence level of the students and their living status are associated. For this the null and alternative hypotheses were as under:

H_0: No relation between confidence level and living location for understanding of mathematical concept of limits.

H_1: Some relation between confidence level and living location for understanding of mathematical concept of limits.

Table 3.1 gives a cross classification of respondent's confidence level by their opinion concerning of understanding of limit concept. Notice that five point confidence level scales has been used with the categories being strongly agree, agree, neither agree nor disagree, disagree and strongly disagree.

The χ^2 table value for 0.05 significance and 4 degrees of freedom gives a critical value of 9.488. At 0.05 significance, the region of rejection of H_0 is all Chi square values of 9.488 or more.

Since 5.612 < 9.488, the Chi square value from the table is in the region of acceptance of the null hypothesis and the null hypothesis of no relationship between confidence level and living status of students can be accepted.

Therefore at the 0.05 level of significance, there is evidence of no relationship between confidence level and living status of students while learning limit concepts.

TABLE 3.1

Association between Confidence Level and Living Status towards Understanding of Limit Concept

Living Status	Confidence Level of Students					Row Total
	Strongly Agree	Agree	Neither	Disagree	Strongly Disagree	
Rural	115	79	10	13	04	**221**
Urban	156	88	17	08	10	**279**
Column Total	**271**	**167**	**27**	**21**	**14**	**500**

Chi-Square	Value	DF	Significance
Pearson	5.612	4	0.230

4. RELATION BETWEEN CURIOSITY AND LIVING STATUS OF STUDENTS TOWARD UNDERSTANDING OF LIMIT CONCEPTS

In this case, respondents (students) were asked their views concerning whether it is an effectible of curiosity along with their residence location to understand the concept of limit concept.

The hypotheses have been made to check whether or not the curiosity level of the students and their living status are associated. For this the null and alternative hypotheses were as under:

H_0: No relation between curiosity level and living location for understanding of mathematical concept of limits.

H_1: Some relation between curiosity level and living location for understanding of mathematical concept of limits.

Table 4.1 gives a cross classification of respondent's curiosity level by their opinion concerning of understanding of limit concept. Notice that three point curiosity level scales has been used with the categories being fully solved, partially solved and not solved.

TABLE 4.1

Association between Curiosity Level and Living Status towards Understanding of Limit Concept

Living Status	Curiosity Level of Students			Row Total
	Fully Solved	Partially Solved	Not Solved	
Rural	93	94	34	**221**
Urban	123	114	42	**279**
Column Total	**216**	**208**	**76**	**500**

Chi-Square	Value	DF	Significance
Pearson	0.564	2	0.902

The χ^2table value for 0.05 significance and 2 degrees of freedom gives a critical value of 5.991. At 0.05 significance, the region of rejection of H_0 is all Chi square values of 5.991 or more.

Since 0.564 < 5.991, the Chi square value from the table is in the region of acceptance of the null hypothesis and the null hypothesis of no relationship between curiosity level and living status of students can be accepted.

Therefore at the 0.05 level of significance, there is evidence of no relationship between curiosity level and living status of students while learning limit concepts.

5. RELATION BETWEEN CONFIDENCE AND GENDER OF STUDENTS TOWARD UNDERSTANDING OF LIMIT CONCEPTS

In this case, respondents (students) were asked their views concerning whether it is an effectible of confidence level along with gender (boy or girl) to understand the concept of limit concept.

The hypotheses have been made to check whether or not the confidence level of the students and their gender status are associated. For this the null and alternative hypotheses were as under:

H_0: No relation between confidence level and gender for understanding of mathematical concept of limits.

H_1: Some relation between confidence level and gender for understanding of mathematical concept of limits.

TABLE 5.1

Association between Confidence Level and Gender Status towards Understanding of Limit Concept

Gender Status	Confidence Level of Students					Row Total
	Strongly Agree	Agree	Neither	Disagree	Strongly Disagree	
Boy	136	87	13	07	07	**250**
Girl	135	80	14	14	07	**250**
Column Total	**271**	**167**	**27**	**21**	**14**	**500**

Chi-Square	Value	DF	Significance
Pearson	2.667	4	0.615

Table 5.1 gives a cross classification of respondent's confidence level by their opinion concerning of understanding of limit concept. Notice that five point confidence level scales has been used with the categories being strongly agree, agree, neither agree nor disagree, disagree and strongly disagree.

The χ^2 table value for 0.05 significance and 4 degrees of freedom gives a critical value of 9.488. At the 0.05 significance, the region of rejection of H_0 is all Chi square values of 9.488 or more.

Since 2.667 < 9.488, the Chi square value from the table is in the region of acceptance of the null hypothesis and the null hypothesis of no relationship between confidence level and gender status of students can be accepted.

Therefore, at the 0.05 level of significance, there is evidence of no relationship between confidence level and gender status of students while learning limit concepts.

6. RELATION BETWEEN CURIOSITY AND GENDER OF STUDENTS TOWARD UNDERSTANDING OF LIMIT CONCEPTS

In this case, respondents (students) were asked their views concerning whether it is an effectible of curiosity along with their gender (boy or girl) to understand the concept of limit concept.

The hypotheses have been made to check whether or not the curiosity level of the students and their gender status are associated. For this the null and alternative hypotheses were as under:

H_0: No relation between curiosity level and gender for understanding of mathematical concept of limits.

H_1: Some relation between curiosity level and gender for understanding of mathematical concept of limits.

TABLE 6.1

Association between Curiosity Level and Gender Status towards Understanding of Limit Concept

Gender Status	Curiosity Level of Students			Row Total
	Fully Solved	Partially Solved	Not Solved	
Rural	100	109	41	**250**
Urban	116	99	35	**250**
Column Total	**216**	**208**	**76**	**500**

Chi-Square	Value	DF	Significance
Pearson	2.140	2	0.343

Table 6.1 gives a cross classification of respondent's curiosity level by their opinion concerning of understanding of limit concept. Notice that three point curiosity level scales has been used with the categories being fully solved, partially solved and not solved.

The χ^2 table value for 0.05 significance and 2 degrees of freedom gives a critical value of 5.991. At the 0.05 significance, the region of rejection of H_0 is all Chi square values of 5.991 or more.

Since 2.140 < 5.991, the Chi square value from the table is in the region of acceptance of the null hypothesis and the null hypothesis of no relationship between curiosity level and gender status of students can be accepted.

Therefore at the 0.05 level of significance, there is evidence of no relationship between curiosity level and gender status of students while learning limit concepts.

7. CONCLUSION

Under the various associations of literacy, confidence and curiosity along with the living status and gender differences among the students were involved under the study. The only alternative hypothesis of literacy of parents has been strongly accepted. In support of what has been observed is by the report of Joint Implementation Committee, IIT Kharagpur (August 2014) clearly made one of the salient feature, "Graduate parents seem to be the majority of qualified candidates (42%) like previous years[4]".

8. ACKNOWLEDGEMENT

This paper is the part of applied research at YCMOU for the fulfillment of the Ph. D. degree in Mathematics in the faculty of science[1].Thanks to reviewers for their constructive comments for improving this paper.

REFERENCES

[1] Adams, R. (2006). Calculus: a complete course. Boston: Pearson Addison Wesley.

[2] Carolyn, A. Lin. (2003). An Interactive Communication Technology Adoption Model: International Communication Association, 13(4), 345-365.

[3] Kristina, Juter. (2006). Limits of Functions, Department of Mathematics. Lulea University of Technology, SE-97187, Lulea

[4] JEE, (2014). (Advanced)-Report, 1, 31.

[5] Yavuz, I. (2010). What does a graphical representation mean for students at the beginning of function teaching? : International Journal of Mathematics Education in Science and Technology, 41(4), 467-485.

[6] Borgen, K.L. & Manu, S.S. (2002). What do students really understand? Journal of Mathematical Behavior, 21(2), 151-165.

[7] Kulkarni M.B., Ghatpande S.B. and Gore S.D. Common Statistical Tests.

Proceedings of 7th National Conference on Multidisciplinary Research in Science & Engineering, MIT AOE Alandi, Pune, 3-4 June 2016, pp. 25-43, ISBN: 978-93-84659-59-2

MATHEMATICAL MODELLING AND CONTROL THEORY ANALYSIS OF ARTIFICIAL SATELLITE

Sonu Lamba
Department of Mathematics, National Institute of Technology Jamshedpur, Jharkhand – 831014, India

Abstract

In this paper, an analysis of Mathematical Control Theory is carried out which concludes controllability of artificial satellites. Control Theory is application-oriented mathematics that deals with the basic principles underlying the analysis and design (control) systems. To control means that one has to influence the behaviour of the system in a desirable way. A preliminary discussion is provided which acts as stairs for reaching final conclusions and includes an analytical approach to model the physical system into dynamical equations of motions which is termed as Mathematical Modelling.

Since most of the real life systems are nonlinear in nature therefore an approach for linearization is described. By doing so, we will able to apply numerous linear analysis methods to study further behaviour of the system. Then a mathematical approach used to compute Transition Matrix for getting solution of linear system by using variation of parameter method.

Throughout the analysis we are looking for minimum norm (optimal) steering controls, after then we made some interesting conclusions by using Kalman's Controllability test.

Finally, a graphical simulation is provided using MATLAB which includes computations of controllability Gramian and controller with related MATLAB codes.

Key Words: Control Theory, Transition Matrix, Optimal Control, Kalman's Controllability test.

1. INTRODUCTION

In today's rapidly progressive environment of Science and Technology, the field of Control Theory is at forefront of the creative interplay of mathematics, engineering and computer science. Control theory is application-oriented Mathematics that deals with the process of influencing the behaviour of a dynamical system so as to achieve a desired goal.
Dynamical System can be engineering systems (Air Conditioner, Aircraft etc.), Economic System, Biological System and so on. To control means that one has to influence the behaviour of the system in a desirable way. For example, in the case of an air conditioner the aim is to control the temperature of a room and maintain it at desired level, while in the case of an aircraft or satellite we wish to control its altitude at each point of time so that it follows a desired trajectory in space or orbit.

Let us discuss some examples to answer the question, what is a control system?

Consider a one dimensional system;

$\frac{dx}{dt}$= - 2x; x(0) = 3.

The solution of the system is x(t) = $3e^{-2t}$ and its graph is given as follows;

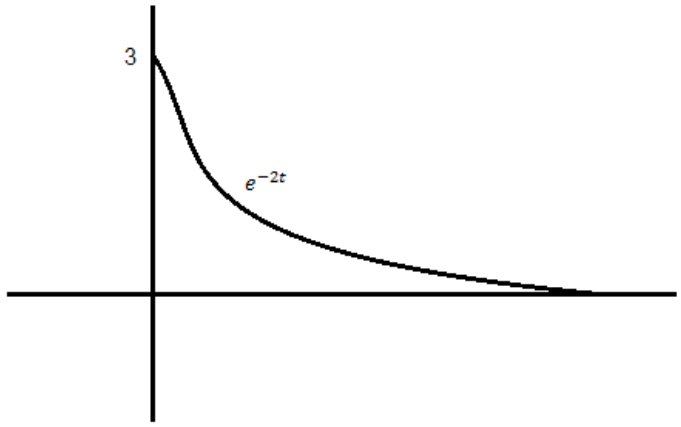

If we add a nonhomogeneous term 'sin(t)' called the forcing term to it then the system is given by

$\frac{dx}{dt}$ = - 2x + sin(t); x(0) = 3.

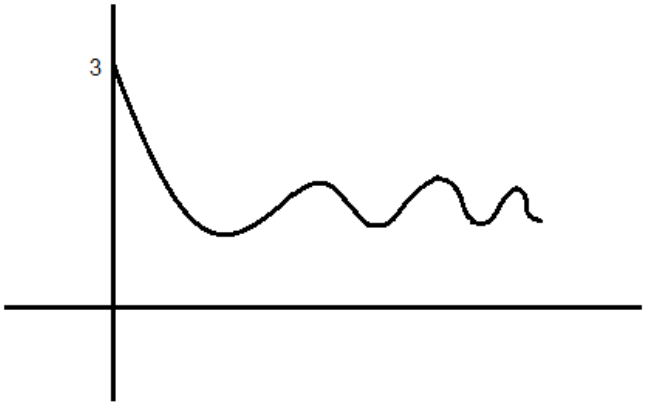

We observe that the solution or the trajectory of the system is changed. This means the evolution of the system is changed by adding the new forcing term to the system. Thus the system with a forcing term is called a control system.

Now we take a tank problem which put out an easy observation of Kalman's controllability test or kalman's rank test;

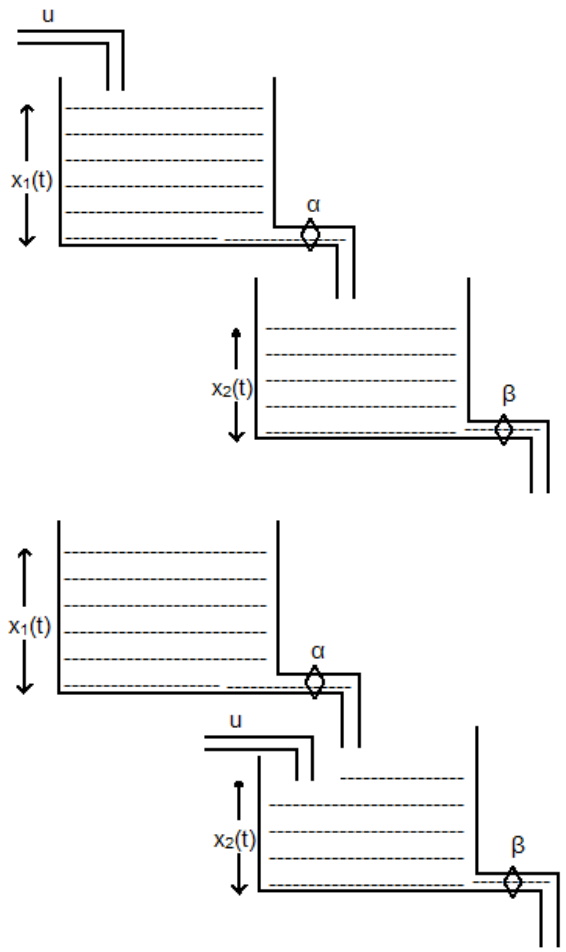

Model 1 Model 2

Let $x_1(t)$ be the water level in tank 1 and $x_2(t)$ be the water level in tank 2. Let 'α' be the rate of outflow from tank 1 and 'β' be the rate of outflow from tank 2. Let 'u' be the supply of water to the system. The system can be modelled (Mathematical Modelling) in following differential equations:

Model 1: $\frac{dx1}{dt} = - \alpha x_1 + u$ (rate of change of water level in tank 1)

$\frac{dx2}{dt} = \alpha x_1 - \beta x_2$ (rate of change of water level in tank 2)

This implies;

$$\frac{d}{dt}\begin{pmatrix} x1 \\ x2 \end{pmatrix} = \begin{pmatrix} -\alpha & 0 \\ \alpha & -\beta \end{pmatrix}\begin{pmatrix} x1 \\ x2 \end{pmatrix} + \begin{pmatrix} 1 \\ 0 \end{pmatrix} u$$

Model 2: similarly, for model 2 we get;

$$\frac{d}{dt}\begin{pmatrix} x1 \\ x2 \end{pmatrix} = \begin{pmatrix} -\alpha & 0 \\ \alpha & -\beta \end{pmatrix}\begin{pmatrix} x1 \\ x2 \end{pmatrix} + \begin{pmatrix} 0 \\ 1 \end{pmatrix} u$$

Obviously the model 2 is not controllable because supply cannot change the water level in tank 1.

Now according to Kalman's controllability test, "If the matrices A and B are time independent then linear system is controllable if and only if

Rank[B AB A^2B.....A^{n-1} B] = n

this matrix is called controllability matrix C." (Discussed in 4.1 section)

here we can easily observe that C = [B: AB] has rank 2 in case of model 1 not in model 2. Hence we can say model 2 is not controllable.

Controllability analysis can be done in many real life problems like biological system, defence systems etc. Here in this paper I produced an analysis of mathematical control theory of artificial satellite using different approaches.

2. MATHEMATICAL MODELLING

2.1. Dynamical Equations of motion

Consider a satellite of mass 'm' orbiting around the earth under inverse square law field. We can assume that the satellite has thrusting capacity with radial thrust 'u_1' and tangential thrust 'u_2'.

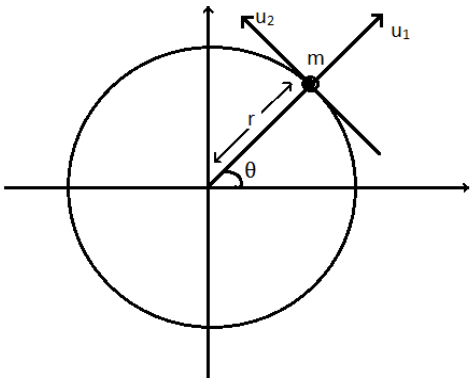

If (x, y) are the rectangular co-ordinates of a particle P of mass m, then the equations of motion are given by

$$\left.\begin{aligned} m\ddot{x} &= f_x \\ m\ddot{y} &= f_y \end{aligned}\right\} \text{----------(1)}$$

where f_x and f_y are components of the force f in directions of the axes. It will be convenient to use polar co-ordinates (r, θ) so that

$$x = r\cos\theta;\ y = r\sin\theta$$

2.2. Equation of motion in Polar coordinate

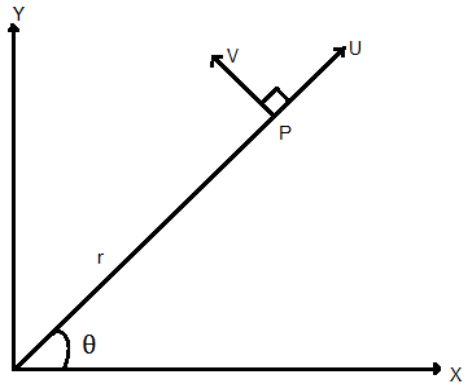

Let u, v denote the components of velocity of the particle P along radial direction $\vec{r}$ and in the tangential direction, respectively.

The resultant of 'u' and 'v' is also the resultant of the components of $\dot{x}$and $\dot{y}$.

Therefore, by resolving parallel to x-axis we get,

$\dot{x}$= u cos θ -v sin θ -------- (3)

Since x = r cos θ, differentiating with respect to time t,

$\dot{x} = \dot{r}\cos\theta - r\sin\theta.\dot{\theta}$ ------- (4)

From (3) and (4) we have

$u\cos\theta - v\sin\theta = \dot{r}\cos\theta - r\sin\theta.\dot{\theta}$ -------- (5)

Comparing coefficient of cos θ and sin θ from Eq. (5) we have:

$u = \dot{r}$ and
$v = r\dot{\theta}$

$u = \dot{r}$ is the radial velocity of P and $v = r\dot{\theta}$ is its transverse component.

Now, if 'a_1' and 'a_2' denote the components of the accelerations alongradial and transverse directions, respectively. Then by resolving itparallel to OX, OY we get,

$\ddot{x} = a_1\cos\theta - a_2\sin\theta$

By Differentiating Eq. (4) we have;

$\ddot{x} = \frac{d\dot{x}}{dt} = \frac{d}{dt}\left(\dot{r}\cos\theta - r\sin\theta\,\dot{\theta}\right)$ --------- (6)

$=\ddot{r}\cos\theta-\dot{r}\sin\theta\dot{\theta}--\dot{r}\sin\theta\dot{\theta}-r\cos\theta\dot{\theta}^2-r\sin\theta\ddot{\theta}$---- (7)

$= (\ddot{r}-r\dot{\theta}^2)\cos\theta -(2\dot{r}\dot{\theta}+r\ddot{\theta})\sin\theta$ -------(8)

Equating values of $\ddot{x}$ obtained above;

$a_1\cos\theta-a_2\sin\theta = (\ddot{r}-r\dot{\theta}^2)\cos\theta -(2\dot{r}\dot{\theta}+r\ddot{\theta})\sin\theta$------ (9)

Comparing coefficients of $\cos\theta$ and $\sin\theta$ from Eq. (9) we have the following expressions:

$a_1 = (\ddot{r}-r\dot{\theta}^2)$

$a_2 = (2\dot{r}\dot{\theta}+r\ddot{\theta}) = \frac{1}{r}\frac{d}{dt}(r^2\dot{\theta})$

The quantities 'a_1' and'a_2'are called the radial and transverse components of acceleration, respectively.

The equation of motion of the particle P can now be written as;

$ma_1 = m(\ddot{r}-r\dot{\theta}^2) = F_r$ and $ma_2 = m\frac{1}{r}\frac{d}{dt}(r^2\dot{\theta}) = F_\theta$ ------- (10)

In the case of central orbits, the force is always directed towards afixed point. If we take this point as the origin, then $F_\theta = 0$. If $F_r = -k/r^2$i.e, inverse square force field such as gravity, then

$$\left.\begin{aligned} m(\ddot{r}-r\dot{\theta}^2) &= -k/r^2 \\ m r\ddot{\theta} + 2\dot{r}\dot{\theta}m &= 0 \end{aligned}\right\} \quad \text{-------- (11)}$$

Assume that the mass is equipped with the ability to exert a thrust 'u_1' in the radial direction and 'u_2' in the tangential direction.Then under the presence of these external forces, the equations of motion become;

$$\left.\begin{aligned} m\ddot{r}-mr\dot{\theta}^2+k/r^2 &= u_1 \\ m r\ddot{\theta} + 2\dot{r}\dot{\theta}m &= u_2 \end{aligned}\right\} \quad \text{--------- (12)}$$

which are required differential equation of dynamical satellite motion.

2.3. State Space Representation of Equations of motion

Assume that the mass 'm' of the satellite is 1 (unit mass). Then, the motion of a satellite is described by a pair of second order differential equations;

$\ddot{r} = r\dot{\theta}^2 - k/r^2 + u_1$ --------- (13)

$\ddot{\theta} = \frac{-2}{r(t)}\dot{r}\dot{\theta} + u_2/r(t)$ --------- (14)

If $u_1 = 0 = u_2$, then one can show that Eq. (13) and Eq. (14) have solutions given by

$r(t) = \sigma$

$\theta(t) = \omega t$

where σ and ω are constant and $\sigma^3\omega^2 = k$.

Make the following change of variables:

$x_1 = r - \sigma$ ------ (15)

$x_2 = \dot{r}$ ------ (16)

$x_3 = \sigma(\theta - \omega t)$ ------ (17)

$x_4 = \sigma(\dot{\theta} - \omega)$ ------ (18)

This gives

$r = x_1 + \sigma$ ------- (19)

$\dot{r} = x_2$ ------- (20)

$\theta = \frac{x3}{\sigma} + \omega t$ ----- (21)

$\dot{\theta} = \frac{x4}{\sigma} + \omega$ ------- (22)

So using the above transformations Eq. (13), (14), reduce to a system of four first order non-linear differential equations:

$\frac{d}{dt}x_1 = x_2$---------- (23)

$\frac{d}{dt}x_2 = (x_1 + \sigma)\left(\frac{x_4}{\sigma} + \omega\right)^2 - k/(x_1 + \sigma)^2 + u_1$ ---------- (24)

$\frac{d}{dt}x_3 = x_4$ ---------- (25)

$\frac{d}{dt}x_4 = -2\sigma\left(\frac{x4}{\sigma} + \omega\right)\frac{x_2}{(x1 + \sigma)} + \frac{u_2\sigma}{(x1 + \sigma)}$ ---------- (26)

The above equations form a system of nonlinear ordinary differential equations involving the forcing functions (controls) 'u_1' and 'u_2' can be written in the compact vector notation as given below:

$\frac{dx}{dt} = f(x, u); \quad \forall\, x(t) \in \mathbb{R}^4,\ u(t) \in \mathbb{R}^2$---------- (27)

Here f is a vector with components f_1; f_2; f_3; f_4 given by;

$$\left.\begin{aligned} f_1(x_1;x_2;x_3;x_4;u_1;u_2)&=x_2 \\ f_2(x_1;x_2;x_3;x_4;u_1;u_2) &= (x_1+\sigma)\left(\frac{x_4}{\sigma}+\omega\right)^2 - k/(x_1+\sigma)^2 + u_1 \\ f_3(x_1;x_2;x_3;x_4;u_1;u_2) &= x_4 \\ f_4(x_1;x_2;x_3;x_4;u_1;u_2) &= -2\sigma\left(\frac{x4}{\sigma}+\omega\right)\frac{x_2}{(x1+\sigma)}+\frac{u_2\sigma}{(x1+\sigma)} \end{aligned}\right\}$$

This is the required State Space Representation of dynamical equations of the satellite motion.

2.4. Linearization of Nonlinear Systems

Most of the differential equations and system of differential equations are encountered in practise are non-linear. And most of the real life problems are based on the non-linear system. But many of times we are unable to solve non-linear differential equation, so we linearize the system to get a linear equation that can be easily solved. So here our first concern is to linearize the non-linear system. After linearizing the non-linear system, we can easily apply the numerous linear analysis methods to study the nature of the system.

Approach to linearization

We now linearize the non-linear system about the zero equilibrium solution to obtain the system in the form of the linear control system

$\dot{x}(t) = Ax(t) + Bu(t)$.

By linearizing the function f (x; u), described above, about x= 0, u=0 we have**;**

$\hat{f}(x, u) = f_x'(0, 0)\, x + f_u'(0, 0)\, u = Ax(t) + Bu(t)$.

where

$$A = f_x'(0, 0) = \begin{pmatrix} \frac{\partial f_1}{\partial x_1} & \frac{\partial f_1}{\partial x_2}\frac{\partial f_1}{\partial x_3} & \frac{\partial f_1}{\partial x_4} \\ \frac{\partial f_2}{\partial x_1} & \frac{\partial f_2}{\partial x_2}\frac{\partial f_2}{\partial x_3} & \frac{\partial f_2}{\partial x_4} \\ \frac{\partial f_3}{\partial x_1} & \frac{\partial f_3}{\partial x_2}\frac{\partial f_3}{\partial x_3} & \frac{\partial f_3}{\partial x_4} \\ \frac{\partial f_4}{\partial x_1}\frac{\partial f_4}{\partial x_2}\frac{\partial f_4}{\partial x_3}\frac{\partial f_4}{\partial x_4} \end{pmatrix} \quad \text{at } (0, 0)$$

$$= \begin{pmatrix} 0 & 1 & 0 & 0 \\ 3\omega^2 & 0 & 0 & 2\omega \\ 0 & 0 & 0 & 1 \\ 0 & -2\omega & 0 & 0 \end{pmatrix} \quad \text{---------- (28)}$$

and

$$B = f_u'(0, 0) = \begin{pmatrix} \frac{\partial f_1}{\partial u_1} & \frac{\partial f_1}{\partial u_2} \\ \frac{\partial f_2}{\partial u_1} & \frac{\partial f_2}{\partial u_2} \\ \frac{\partial f_3}{\partial u_1} & \frac{\partial f_3}{\partial u_2} \\ \frac{\partial f_4}{\partial u_1} & \frac{\partial f_4}{\partial u_2}(0,0 \quad) \end{pmatrix} = \begin{pmatrix} 0 & 0 \\ 1 & 0 \\ 0 & 0 \\ 0 & 1 \end{pmatrix} \text{---------- (29)}$$

Here σ is normalized to 1. So the linearized system thus obtained is

$\dot{x}(t) = Ax(t) + Bu(t)$.

where A and B are given by Eq. (28) and Eq. (29) respectively.

2.5. Transition Matrix and solution of Linear System

We now consider a more general homogeneous linear system:

$\dot{x}$= A(t)x, $x(t_0) = x_0$ ---------- (30)

where A(t) is an n x n matrix whose entries are continuous functions of t.

- The system (30) has a unique solution for any initial state $x_0 \in \mathbb{R}^n$.
- The set of all solutions of the system forms an n dimensional vector space.
- A set of n-linearly independent initial states in $\mathbb{R}^n$ will provide a set of n- linearly independent solutions of the system.

In this section we will present a brief description of Transition matrix with its computational techniques and solution of linear system.

2.5.1. Definition of Transition Matrix

Let $\{e_1, e_2, e_3, \ldots\ldots, e_n\}$ be the canonical basis in $\mathbb{R}^n$.

Let $\varphi_k(t)$ denotes the unique solution of the following initial value problem for each fixed k.

$\dot{x}$= A(t)x, $x(t_0) = e_k$ ---------- (31)

We now define a matrix (called Transition Matrix) $\varphi(t; t_0)$ by using these n-linearly independent solutions of the system (30).
The n x n matrix $\varphi(t; t_0)$ defined by:

$$\varphi(t; t_0) = [\varphi_1(t), \varphi_2(t), ..., \varphi_n(t) \ ] \text{ ---------- (32)}$$

is called Transition Matrix.

2.5.2. Properties of transition matrix

Let $\varphi(t; t_0)$ be the transition matrix for the linear system $\dot{x} = A(t)x$.

Then $\varphi(t; t_0)$ satisfies the following properties;

- $\varphi(t; t) = I$
- $\varphi(t; t_0)\, \varphi(t_0; s) = \varphi(t; s)$
- $\varphi(t; t_0)^{-1} = \varphi(t_0; t)$
- $\frac{\partial \varphi(t; t_0)}{\partial t} = -\varphi(t; t_0)\, A(t_0)$

2.5.3. Computation of transition matrix

In this section we discuss about computation techniques of transition matrix. We take both cases that when matrix A is diagonalizable and when matrix A is not diagonalizable.
For the time-invariant system $\dot{x} = A(t)x$, the transition matrix can be written in the matrix exponential form:

$$\varphi(t; t_0) = e^{A(t-t_0)}$$

Computation of e^{At} :
Case 1:

If the matrix A is diagonalizable. Then there exists a matrix P of the eigenvectors of A such that

$$A = PDP^{-1}$$

where D is the diagonal matrix containing eigenvalues of A. Then,

$$e^{At} = 1 + At + ...+ \frac{A^n t^n}{n!} + ...$$

$$= P[1 + Dt + ... + \frac{D^n t^n}{n!} + ... \ ] P^{-1}$$

$$= P\, e^{Dt} P^{-1} \qquad \text{---------- (33)}$$

Case 2:

When A is not diagonalizable. Let be $\lambda_1, \lambda_2, \lambda_3, ... \lambda_n$ be the eigenvalues of A with algebraic multiplicities $m_1, m_2, m_3, ...m_k$ respectively. Then,

$n = m_1 + m_2 + m_3 + ... + m_k$.

Let X_k be the soluton space of $(A - \lambda_k)^{m_k} x = 0$ Decomposing $\mathbb{C}^n$ using these spaces we have;

$\mathbb{C}^n = X_1 + X_2 + ... + X_k$

Let $x_0 \in \mathbb{C}^n$ then x_0 has unique decomposition

$x_0 = x_{01} + x_{02} + ... + x_{0k}$ with $x_{0j} \in x_j$.

Then we have the following:

$$e^{At}x_0 = \sum_{j=1}^{k} e^{At}\, x_{0j}$$

$$= \sum_{j=1}^{k} e^{\lambda_j t}\, e^{(A-\lambda_j I)t} x_{0j}$$

$$= \sum_{j=1}^{k} e^{\lambda_j t} \left[1 + t(A - \lambda_j I) + ... + \frac{t^{m_j-1} t^n}{m_j - 1!}(A - \lambda_j I)^{m_j - 1}\right] x_{0j}$$

$$= \sum_{j=1}^{k} e^{\lambda_j t} \left[\sum_{i=0}^{m_i - 1} \frac{t^i}{i!}(A - \lambda_j)^i\right] x_{0j} \qquad \text{-------- (34)}$$

Equation (33) and (34) represents the computed formulae for transition matrix.

Example: Let $\dot{x} = Ax$ be the given system, where A is,

$A = \begin{bmatrix} -1 & 3 \\ 0 & 2 \end{bmatrix}$; A has eigen values $\lambda_1 = -1$, $\lambda_2 = 2$

And the eigen vectors of A are $\begin{bmatrix} 1 \\ 0 \end{bmatrix}$ and $\begin{bmatrix} -1 \\ 1 \end{bmatrix}$ corresponding to eigen values -1 and 2 respectively.Therefore, A can be written as

$A = PDP^{-1}$, where P and D are given by the following matrices.

$P = \begin{bmatrix} 1 & -1 \\ 0 & 1 \end{bmatrix}$ and $D = \begin{bmatrix} -1 & 0 \\ 0 & 2 \end{bmatrix}$

Now; $e^{At} = P\, e^{Dt} P^{-1}$ that is,

$$e^{At} = \begin{bmatrix} 1 & -1 \\ 0 & 1 \end{bmatrix} \begin{bmatrix} e^{-t} & 0 \\ 0 & e^{2t} \end{bmatrix} \begin{bmatrix} 1 & 1 \\ 0 & 1 \end{bmatrix}$$

Thus

$$e^{At} = \begin{bmatrix} e^{-t} & e^{-t} - e^{2t} \\ 0 & e^{2t} \end{bmatrix}$$

2.5.4. Solution of Linear System

By using the variation of parameter method the solution of the non-homogeneous system

$\dot{x}(t) = Ax(t) + Bu(t)$ can be written in the form:

$$X(t) = \varphi(t; t_0)\, x_0 + \int_{t_0}^{t} \varphi(t; \tau) Bu(\tau) d(\tau)$$

where, $\varphi(t; \tau)$ is the transition matrix for the homogeneous system.

3. CONTROLLABILITY OF LINEAR SYSTEMS

3.1. Definition and Introduction

The dynamical system $\dot{x}(t) = Ax(t) + Bu(t)$ with initial condition $x(t_0) = x_0$ is said to be controllable during the time interval $[t_0; t_1]$ if for every x_0, x_1 in $\mathbb{R}^n$ there exists a controller $u \in L^2([t_0; t_1]; \mathbb{R}^m])$ such thatthe corresponding solution starting from $x(t_0) = x_0$ also satisfies thedesired final state $x(t_1) = x_1$.

The controllability problem is to check the existence of a forcing term or control function u(t) such that the corresponding solution of the system will pass through a desired point $x(t_1) = x_1$.

We now show that the scalar control system

$\dot{x}(t) = Ax(t) + Bu(t); \quad x(t_0) = x_0$

is controllable. We produce a control function u(t) such that the corresponding solution starting with $x(t_0) = x_0$ also satisfies $x(t_1) = x_1$. Choose a differentiable function z(t) satisfying $z(t_0) = x_0$ and $z(t_1)=x_1$:-

For example, by the method of linear interpolation,

$z - x_0 = \frac{(x_1 - x_0)}{(t_1 - t_0)} (t - t_0)$

Thus the function

$Z(t) = x_0 + \frac{(x_1 - x_0)}{(t_1 - t_0)} (t - t_0)$

which satisfies both $z(t_0) = x_0$; $z(t_1) = x_1$

3.2. Computation of steering controls

For the linear system

$\dot{x}(t) = Ax(t) + Bu(t)$ with initial condition $x(t_0) = x_0$,

we are looking for controller 'u', which will steer the system to x_1 during time-interval $[t_0; t_1]$. That is, the corresponding solution should satisfy $x(t_1) = x_1$. We know that:

$x(t_1) = x_1 = \varphi(t_1; t_0)\, x_0 + \int_{t_0}^{t_1} \varphi(t_1; t) Bu(t) dt.$

$x_1 - \varphi(t_1; t_0)\, x_0 = \int_{t_0}^{t_1} \varphi(t_1; t) Bu(t) dt$ ---------- (35)

Define an operator $C: L^2([t_0; t_1]; \mathbb{R}^m) \to \mathbb{R}^n$ by,

$Cu = \int_{t_0}^{t_1} \varphi(t; \tau) Bu(\tau) d(\tau)$ ---------- (36)

Obviously C is a bounded linear operator.

Define a vector $d = x_1 - \varphi(t_1; t_0)\, x_0$; so using (36) the Eq. (35) becomes,

$Cu = d$ ---------- (37)

If the operator C is onto then the system is controllable.

RESULT: The following conditions are equivalent;

- The system is controllable.
- The operator C is onto.
- The operator CC^T: $\mathbb{R}^n \to \mathbb{R}^n$ is onto.

The operator CC^T is called controllability Grammian and is given by:

$$w(t_1; t_0) = \int_{t_0}^{t_1} \varphi(t; \tau) B(\tau) B^T(\tau)\, \varphi^T(t; \tau) d(\tau)$$

We are looking for the solution u of the operator equation (37);

$Cu = d$ ---------- (38)

Consider an associated operator equation,

$CC^T v = d$ ---------- (39)

where, $u = C^T v$ for some $v \in \mathbb{R}^n$. If the controllability Gramian is invertible then we have,

$v = (CC^T)^{-1} d$

so steering control u is given by,

$u = C^T v = C^T (CC^T)^{-1} d$,

by putting the values of C and d we get;

$u(t) = B^T(t) \varphi^T(t_1; t) w^{-1}(t_0; t_1)(x_1 - \varphi(t_1; t_0)\, x_0)$

which is required control for the system.

RESULT: The following conditions are equivalent for the linear time invariant system $\dot{x} = Ax + Bu$

- The system is controllable.
- rank[B AB A^2B.....A^{n-1} B] = n (this matrix is called controllability matrix C).
- No eigenvector of A^T in kernel of B^T.
- Eigenvalues of [A+BK] can be placed arbitrarily for some suitable choice of K,this is equivalent to complete stabilizability of system.
- rank[$A - \lambda\ I$ B] = n for every eigen value λ of A.

4. CONCLUSIONS ON CONTROLLABILITY

Here are the main conclusions of controllability of satellite problem for which we have studied above topics. In this section we basically describe the conclusion made by Kalman's controllability test and effects of thrusters or controllers on controllability of satellite in orbit of motion.

We have already studied in 2.4. section that the linearized equation of motion of satellite problem is given by

$\frac{dx}{dt}$ = Ax(t) + Bu(t)

Where, $x = (x_1, x_2, x_3, x_4)^T$, $u = (u_1, u_2)^T$ and

$$A = \begin{pmatrix} 0 & 1 & 0 & 0 \\ 3\omega^2 & 0 & 0 & 2\omega \\ 0 & 0 & 0 & 1 \\ 0 & -2\omega & 0 & 0 \end{pmatrix}, \quad B = \begin{pmatrix} 0 & 0 \\ 1 & 0 \\ 0 & 0 \\ 0 & 1 \end{pmatrix}$$

4.1. Kalman's controllability test

Statement: "If the matrices A and B are time independent then linear system is controllable if and only if; Rank[B AB A^2B.....A^{n-1} B] = n

this matrix is called controllability matrix C."

For the linearized satellite system, we can easily compute thecontrollability matrix C;

C = [B: AB: A^2B: A^3B]

It is given by,

$$C = \begin{pmatrix} 0 & 0 & 1 & 0 & 0 & 2\omega & -\omega^2 & 0 \\ 1 & 0 & 0 & 2\omega & -\omega^2 & 0 & 0 & -2\omega^3 \\ 0 & 0 & 0 & 1 & -2\omega & 0 & 0 & -4\omega^2 \\ 0 & 1 & -2\omega & 0 & 0 & -4\omega^2 & 2\omega^3 & 0 \end{pmatrix}$$

We can verify that rank of C is 4 and hence the linearized motion of the satellite is controllable.

4.2. Effect of controllers or thrusters on controllability

It is interesting to ask the following question:-

"What would happen if one of the controllers or thrusters becomes in-operative?"

Here "in-operative" means either u_1 (radial thrusters) or u_2 (tangential thrusters) fails to act on motion of satellite that is one of them become zero.

Case1: First we set $u_2 = 0$ and hence B reduces to $B_1 = [0\ 1\ 0\ 0\ \ ]^T$,

So the controllability matrix $C_1 = [B_1: AB_1: A^2B_1: A^3B_1]$ and is given by;

$$C_1 = \begin{pmatrix} 0 & 1 & 0 & -\omega^2 \\ 0 & 0 & -\omega^2 & 0 \\ 0 & 0 & -2\omega & 0 \\ 0 & -2\omega & 0 & 2\omega^3 \end{pmatrix}$$

As C_1 has rank 3, and the system is not controllable with the radial thrusters alone.

Case2: On other hand when the radial thrusters fail that is, $u_1 = 0$.
In that case B reduces to $B_2 = [0\ 0\ 0\ 1\quad]^T$, and this gives controllability matrix

$C_2 = [B_2: AB_2: A^2B_2: A^3B_2]$, as;

$$C_2 = \begin{pmatrix} 0 & 0 & 2\omega & 0 \\ 0 & 2\omega & 0 & -2\omega^2 \\ 0 & 1 & 0 & -4\omega^2 \\ 1 & 0 & -4\omega^2 & 0 \end{pmatrix}$$

Here C_2 has rank 4 so the absence of radial thrusters doesn't affect the controllability of the system that is system is controllable.

RESULT: Hence by observing both cases we can say that "the loss of radial thrusters doesn't destroy the controllability of the satellite, whereas the loss of tangential thrusters do."

5. MATLAB SIMULATION AND CONCLUSIONS

MATLAB ("MATrix LABoratory") is a tool for numerical computation and visualization. The basic data element is a matrix, so if you need a program that manipulates array-based data it is generally fast to write and run in MATLAB.
Here in this section, we just compute a steering controller which steers the linearized satellite system from the initial state $x_0 = [1; 2; 3; 4]^T$ to a desired final state $x_1 = [4; 3; 2; 1]^T$ by using the control given by

$$u(t) = B^T(t)\varphi^T(t_1; t)w^{-1}(t_0; t_1)(x_1 - \varphi(t_1; t_0)x_0)$$

The computation is carried out in MATLAB with $\omega = 1$ and $t_1 = 1$. Thetransition matrix and the controllability Grammian are computed inside the MATLAB codes.

5.1. MATLAB Codes

```
%Satellite Problem
    clear
    clc
    disp('Linear System dot(x) = Ax + Bu where A and B are given as
    follows:')
    A = [0 1 0 0;3 0 0 2;0 0 0 1;0 -2 0 0]
    B = [0 0;1 0;0 0;0 1]

    disp('The controllability Matrix of the system is:')
    n = size(A,1);
    nu = size(B,2);

    co = zeros(n,n*nu);
    co(:,1:nu) = B;
    for k=1:n-1
    co(:,k*nu+1:(k+1)*nu) = A * co(:,(k-1)*nu+1:k*nu);
    end
    mat=co
```

```
    disp('The rank of the controllability matrix is:')
    ran=rank(mat)
    if ran==0
    disp('The system is controllable')
    else
    disp('The system is not controllable')
    end

    t = sym('t');
    s = sym('s');
    disp('The initial state is:')
    x0 = [1;2;3;4]

    disp('The final state is:')
    x1 = [4;3;2;1]

    disp('We want to to reach the final state in time')
    T = input('Enter the final time:')

    disp('The controllability Gramian is:')
    W = int((expm(A*(T-t))*B*B'*expm(A'*(T-t))),t,0,T);
    subs(W)

    disp('The controller is taken as:')
    u = B'*expm(A'*(T-t))*inv(W)*(x1-expm(A*T)*x0)
    U=subs(u,s);
    disp('The solution of the system using the above controller is:')
    x =(expm(A*t))*x0 + int(expm(A*(t-s))*B*U,s,0,t)

    disp('The Graph of the solution is:')
    z=linspace(0,T,100);
    xt1=subs(x(1),z);
    xt2= subs(x(2),z);
    xt3= subs(x(3),z);
    xt4= subs(x(4),z);
    figure
    plot(z,xt1,z,xt2,z,xt3,z,xt4)
    %for computing the controllers data
    ut1=subs(u(1),z);
    ut2= subs(u(2),z);
    figure
plot(z,ut1,'r',z,ut2,'g')
```

5.2. MATLAB Computations

The MATLAB codes to compute the controllability grammian andcontroller are given below.

To compute Grammian W(0; 1), we use the code line:

```
disp('The controllability Gramian is:')
    W = int((expm(A*(T-t))*B*B'*expm(A'*(T-t))),t,0,T);
```

To compute controller, we use the code line:

```
    disp('The controller is taken as:')
    u = B'*expm(A'*(T-t))*inv(W)*(x1-expm(A*T)*x0)
```

The computed controllability Grammian W(0; 1) is given by:

$$W(0,1) = \begin{pmatrix} 0.4502 & 0.7764 & -0.0754 & -0.5834 \\ 0.7767 & 1.8180 & 0.1461 & -0.6340 \\ -0.0754 & 0.1461 & 0.3123 & 0.4896 \\ -0.5834 & -0.6340 & 0.4896 & 1.5326 \end{pmatrix}$$

*These are the main computations carried by MATLAB. It's not possible to write all the calculations because it will take a numbers of pages.

5.3. MATLAB Graphs

5.3.1. The following graph shows the controlled states of linearized satellite system

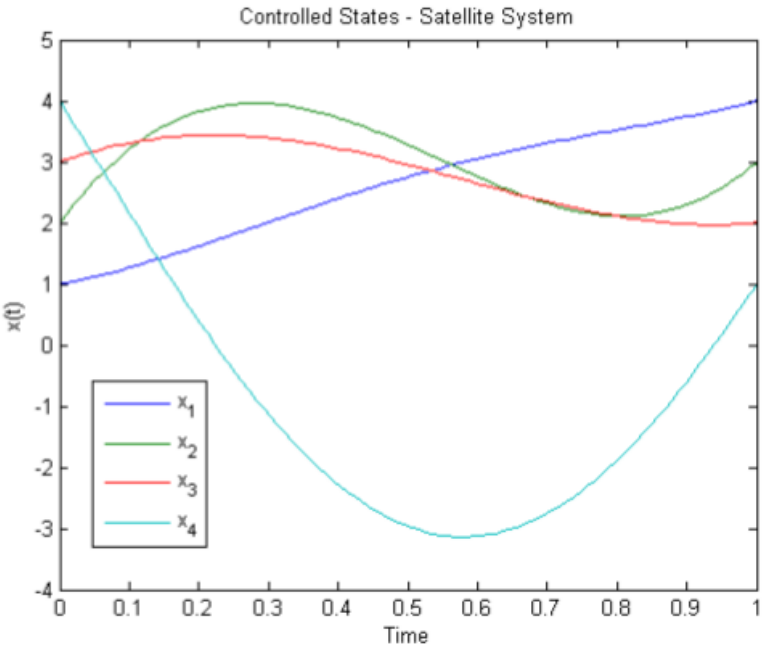

5.3.2. The following graph shows the Steering Control Profile of linearized satellite system.

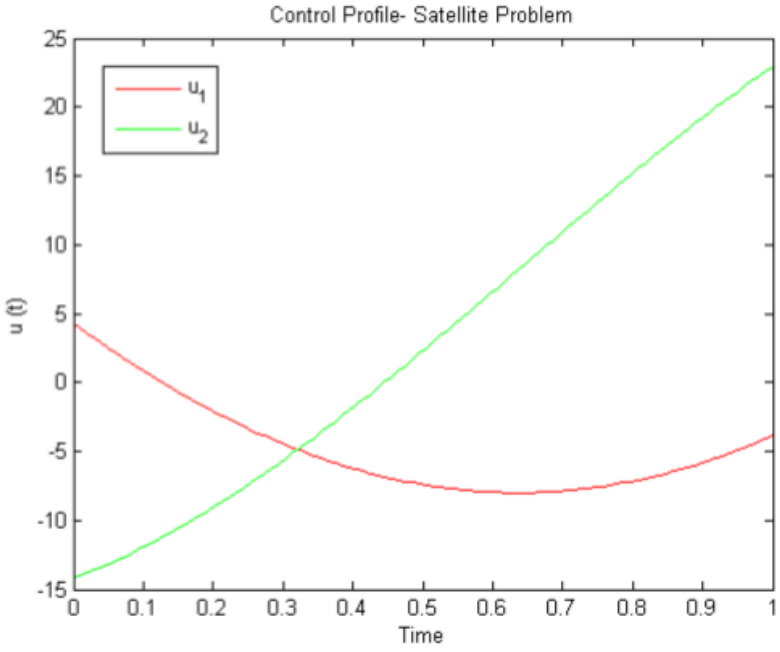

ACKNOWLEDGEMENT

I am ineffably indebted to **Prof. Raju K. George**, Dean (R&D), Sr. Professor and Head, Department of Mathematics, Indian Institute of Space Science and Technology(IIST), Trivandrum for their conscientious guidance to accomplish this work under umbrella of NPDE TCA (Dept. of Mathematics IIT Bombay) sponsored by DST Govt. of India. I extend my gratitude to **Dr. Govindraj Venkatesan**, PDF, Department of Mathematics, IIST, Trivandrum for guiding me.

I am extremely thankful and pay my gratitude to **Dr. Ramayan Singh (HoD)**, **Dr. Ashish Kumar Prashad**, and all other faculty members of Mathematics Department, NIT Jamshedpur to provide a support in writing this paper.
I also acknowledge with a deep sense of reverence, my gratitude towards my parents especially to my respected elder brother **Mr. Bhupender Lamba,** Pupil (Chemical Textiles) at RTU Kota, Rajasthan (India), who has always supported me morally and economically.
My heartiest gratitude goes to my best friend **Miss. Jagriti Gupta,** M.Sc. Scholar Mathematics, University of Delhi and all of my friends who directly or indirectly helped me.
Above all I thank **God** for blessings which enable me to completing my paper.

REFERENCES

[1] Glenn Marion and Daniel Lawson, “An Introduction to Mathematical Modelling” Bioinformatics and Statistics, Scotland, 2008.

[2] K. Balachandran and J.P. Dauer, “Elements of Control Theory”, New Delhi, Narosa Publication, 2012; PP. 40-56.

[3] J. Zabczyk, “Mathematical Control Theory; An Introduction”, Birkhauser Boston.

[4] Joshi M.C. and George R.K., “Controllability of nonlinear System” 1989; PP. 134-166.

[5] George R.K., “Observability of a class of nonlinear abstract system in Mathematical Theory of Control”, edited by M.C. Joshi and A.V. Balakrishnan, Marcel Dekker Inc. New York 1992; PP. 143-160

[6] Amol Sasane, “Calculus of Variations and Optimal Control” 6 Sept 2004; PP. 1-49.

[7] Simmons, George Finlay, “Differential Equations with Application and Historical Notes, New Delhi, Tata Mc Graw-Hill, 2003.

Proceedings of 7th National Conference on Multidisciplinary Research in Science & Engineering, MIT AOE Alandi, Pune, 3-4 June 2016, pp. 44-58, ISBN: 978-93-84659-59-2

COMPARISON OF EXTRACTIVE DISTILLATION AND PRESSURE-SWING DISTILLATION FOR IPA/WATER SEPARATION

Pravin D. Ghuge[1], Nilesh A. Mali[2] and Rajkumar S. Sirsam[1]
[1]Department of Chemical Engineering, University Institute of Chemical Technology, North Maharashtra University, Jalgaon- 425 001(MS),India.
[2]Chemical Engineering & Process Development Division CSIR-National Chemical Laboratory Dr. Homi Bhabha Road, Pune-411008 (MS), India

Abstract

The binary mixture of IPA-Water exhibits a minimum boiling azeotrope with 67.28 mol% IPA at 80.18 C under atmospheric pressure. In this paper, two design alternatives of the distillation processes for separation of IPA-Water azeotropic mixture are investigated. The steady-state simulations are carried out with Aspen Plus Simulator. The comparison in terms of steady-state design is done between extractive distillation of IPA-Water by using DMSO as an entrainer and pressure-swing distillation.

When the purities of the two product streams are set at specified value, it is revealed that the extractive distillation process is significantly more attractive from the standpoint of view of both economical and energy consumption as compared to the pressure-swing distillation. But pressure-swing distillation avoids the potential problem of product contamination due to the extractive solvent that must be added to the binary system.

Key Words: Pressure-swing distillation, extractive distillation, Azeotrope, Distillation design.

1 INTRODUCTION

Isopropyl alcohol (IPA) is mostly used as a solvent in medicine and electronic industries and as a raw material in the paints or ink products. It is also used in the semiconductor industry as a cleaning agent, so the recovery of this cleaning agent from the waste solvent stream is very important. Usually, this waste solvent stream contains mainly isopropyl alcohol (IPA) and water which forms a minimum-boiling azeotrope with a composition of about 67.28 mol % IPA and water at 32.72 mol % at 1 atm. and 80.18 °C temperature. Therefore, a high purity IPA product cannot be obtained through conventional distillation it needs the special distillation.

There are several methods to separate the azeotropic mixtures with or without addition of the entrainer or the solvent. It mainly includes the Extractive distillation, Heteroazeotropic distillation and pressure–swing distillation (Luyben and Chien, 2011; Doherty and Malone, 2001). Heteroazeotropic distillation includes dehydration of isopropyl alcohol and ethanol using cyclohexane or benzene as an entrainer (Chien et al., 2004; Cho et al., 2006),while the extractive distillation of azeotropic mixture like acetone-methanol, IPA-water with heavy entrainers is explained by Luyben (2011).

Pressure-swing distillation can be applied to both and maximum boiling and minimum boiling homogeneous azeotropic mixtures. In minimum boiling azeotropic systems, the distillate streams are recycled, while in maximum boiling azeotropic systems, the bottoms streams are recycled. Pressure- swing distillation is also the attractive option in the separation of azeotropic mixtures such as acetone-methanol, THF-water (Luyben, 2011).

In this paper, extractive distillation of IPA water mixture by using DMSO as an entrainer and pressure swing distillation separation of IPA-Water azeotropic mixture are investigated. The steady-state simulations are carried out with Aspen Plus Simulator. The comparison in terms of steady-state design is done between extractive distillation and pressure-swing distillation to find out the economically feasible method for the separation of IPA water azeotropic mixture

2 EXTRACTIVE DISTILLATION

In extractive distillation, separation is achieved by adding heavy entrainer or solvent, which alters the relative volatility of the original components. Entrainer selection is an important step in extractive distillation before designing a distillation sequence. Certain guidelines should be followed to find out a suitable entrainer for separation of the given azeotropic mixtures. The entrainer must have some special characteristics to achieve the desired separation like thermal stability, higher boiling point, low toxicity, easy recoverability, and suitable change in the relative volatility between the key components (Yuan et al., 2015).

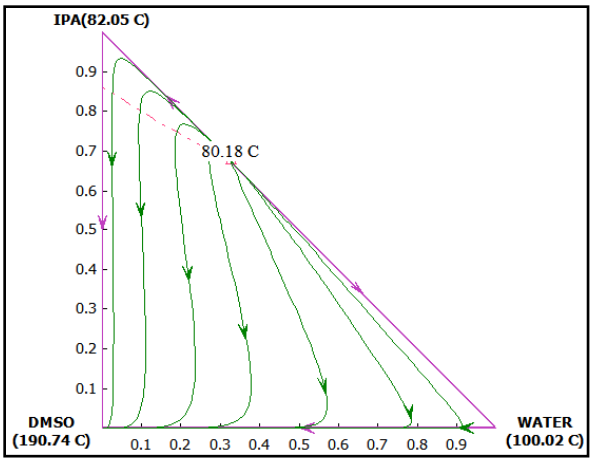

Fig. 1 RCM and Isovolatility curve for IPA-Water-DMSO system at 1 atm.

The residue curve maps are a useful tool to compare different separating agents (entrainer or solvent) in azeotropic and extractive distillation. A Residue Curve Map (RCM) can be used for designing the distillation sequences in extractive distillation. The RCM and isovolatility curves for the IPA-water-DMSO system at 1 atm are shown in Fig. 1. From the RCM, it is clear that DMSO is a feasible entrainer for the IPA-water separation because RCM does not exhibit any distillation boundary.

Isovolatility curve is the locus of the point at which relative volatility of the IPA and water is equal to one. From isovolatility curves in Fig. 1, it was noticed that IPA will come out as distillate from the extractive distillation column because the isovolatility curves intercepts the IPA-DMSO edge of the triangle.

2.1 Aspen Simulation of the IPA-Water Extractive Distillation system

Complete simulation of IPA water azeotropic mixture by using DMSO as an entrainer via extractive distillation is simulated with the help of aspen plus simulator. The product specifications were set to be 99.999 mol % of IPA in distillate as high purity of IPA is required for industrial use. The feed composition considered to be like in typical waste stream in the semiconductor industry containing nearly equimolar IPA and water. The feed flow rate was assumed to be 100 kmol/h and the operating pressure was kept at atmospheric condition, without considering column pressure drop in the Aspen simulation.

To find the optimum operating conditions for the extractive distillation, a sensitivity analysis was performed. The various parameters investigated were as follows: number of stages (NS), Molar reflux ratio (RR), binary feed stage number (NBF), entrainer feed stage number (NEF) entrainer to feed molar ratio (E/F) and temperature of entrainer feed (TEF) . Sensitivity analysis results were used to investigate the influence of above parameter on product composition and heat duties of the column. From the results obtained for the sensitivity analysis, the best operating conditions for the extractive distillation column and solvent recovery column are as listed in the Table 1 and 2 respectively. These results were used in the complete simulation of extractive distillation process.

Table1 EDC operating parameter

Parameter	**Value**
Number of stages	41
Binary feed stage number	33
Entrainer feed stage	6
Molar reflux ratio	0.7
Entrainer to feed molar ratio	1
Temperature of entrainer feed (°C)	75

Table2 SRDC optimum operating parameters

Parameter	**Value**
Number of stages	20
Distillate mole flow (kmol/h)	50
Feed stage number	7
Reflux ratio	0.4
Bottoms temperature (°C)	190
Distillate temperature (°C)	100

The solvent recovery column design was initially done by means of shortcut column calculation (DSTWU) to generate initial guesses for the rigorous simulation (RadFrac) model which was then optimized to establish the molar reflux ratio, feed stage, number of stages and distillate molar flow (kmol/h).

The complete process flow sheet of the IPA-Water extractive distillation sequence with both, extractive and solvent recovery column, simulated in Aspen plus is as given in Fig. 2. Tables 3 and 4 show the inlet feed streams specifications and configuration for the extractive and recovery columns, respectively. The simulation results showed that the obtained IPA mole composition in the extractive column top is 99.999mol%, whereas the water mole composition in the distillate of solvent recovery column is 99.99 mol%. The energy consumption on both extractive and recovery columns is presented in Table 6.

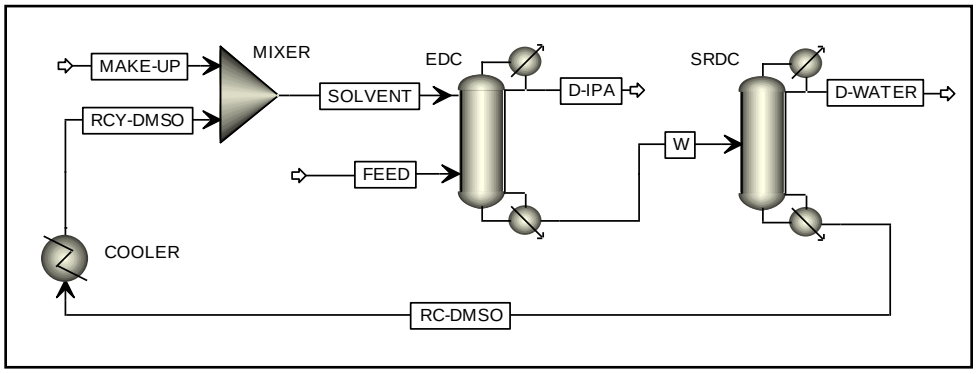

Fig. 2 Complete process flow-diagram for extractive distillation of IPA-Water by using DMSO as an entrainer.

Table 3 Inlet feed streams conditions

Stream Name	Feed	Solvent
Feed mole flow (kmol/h)	100	100
Temperature (ºC)	25	75
Pressure (atm)	1	1
Mole fraction of binary feed IPA Water DMSO 	 0.5 0.5 0	 0 0 1

Table 4 Configuration of EDC and SRDC

Parameter	EDC	SRDC
Number of stages	41	20
Feed stage	33	7
Entrainer feed stage	6	---
Molar reflux ratio	0.7	0.4
Condenser	Total	Total
Pressure (atm)	1	1
Distillate flow (kmol /h)	50	50

Table 5 Simulation Results for complete process flow-diagram for extractive distillation of IPA Water using DMSO as an entrainer

Stream Name	Temperature (°C)	Total mole flow (kmol / h)	IPA (mole fraction)	Water (mole fraction)	DMSO (mole fraction)
FEED	25	100	0.5	0.5	0
SOLVENT	74.99	100	1.8101e-20	9.99953 e-07	0.99999
D-IPA	82.05	50	0.99999	6.44357 e-06	3.55643 e-06
W	143.48	150	3.3333 e-06	0.33333	0.66666
D-Water	100.01	50.0047	9.9990 e-06	0.9999	9.00009 e-05
RE-DMSO	190.74	99.9953	1.8102 e-20	1 e-06	0.99999
RCY-DMSO	75	99.9953	1.8102 e-20	1 e-06	0.99999
MAKE-UP	25	0.00468	0	0	1

Table 6 Condenser and Reboiler Heat Duties on the Columns

	EDC	SRDC
Condenser (kW)	883.47	829.97
Reboiler (kW)	1412.80	1061.08
Cooler (kW)	510.13	

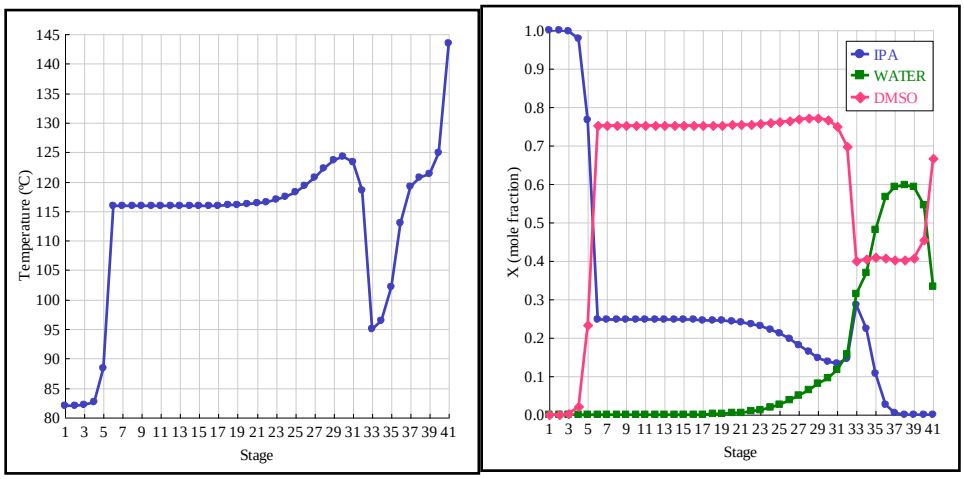

(a) **(b)**

Fig. 3 (a) Temperature profile and **(b)** Liquid-phase composition profiles of EDC.

The temperature profile in the extractive distillation column is shown in Fig.3 (a). Temperature changes at stage 6 due to introduction of the entrainer at this stage. Whereas, at stage number 33 the temperature fluctuation is because of the binary liquid mixture feed on this stage. A significant temperature increase was observed at stages 40 and 41 because of the reboiler proximity.

Liquid-phase composition profiles of IPA, Water, and DMSO in the extractive distillation column is shown in Fig. 3 (b). The main product at the top stage of the column is almost pure IPA and in the bottoms contains the mixture of water and DMSO. It can be seen that the IPA mole fractions increases greatly at stage 6, where an entrainer was fed. The DMSO composition profile has two significant changes at stage number 33 and 6, where the feeds were provided. On the stages between entrainer feed and binary mixture feed, it tends to be constant, as DMSO is less volatile than the other two components; so it is always present in the liquid phase in extractive column. Water shows only significant change at stage 33 at which the binary mixture was fed.

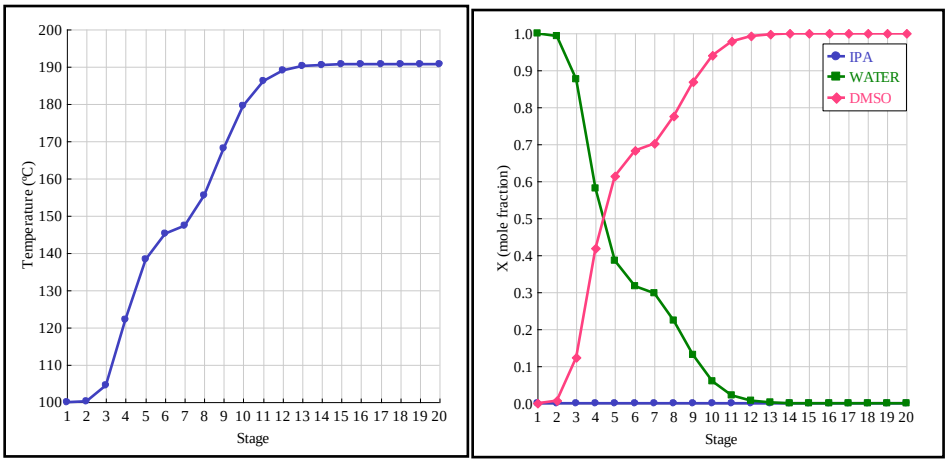

(a) **(b)**

Fig. 4 (a) Temperature profile and **(b)** Liquid-phase composition profile of SRDC.

Temperature profiles and Liquid-phase composition profiles of IPA, Water and DMSO in the solvent recovery column are given in Fig. 4 (a) and (b), respectively. It can be seen from the Fig. 4 (b) that from the top stage of the recovery column almost pure water taken as product while from the bottom pure DMSO taken which was recycled to the extractive column. But from Fig. 4 (a), it was observed that the bottom temperature of solvent recovery column was more than inlet temperature of solvent and due to this solvent was cooled in cooler before recycled back to the extractive column.

2.2 Economical analysis

The economical analysis of the extractive distillation system was evaluated in terms of Total Annual Cost (TAC). It is defined as the sum of energy costs require and annual cost of capital (total capital investment divided by a payback period). The diameter of a distillation column was determined by the 'Tray Sizing' option in Aspen Plus Simulator by assuming sieve tray. The basis of economics and equipment sizing relationships used, which were proposed by Luyben (2013). Table 7 gives TAC of two-column extractive distillation sequence. Total capital investment was estimated to be $\$0.6106\times10^6$. Annual energy cost was 0.6969×10^6 $ per year, using medium pressure steam in the reboiler of the EDC and high pressure steam in the reboiler of the second column that is SRDC.

Table 7 TAC of extractive distillation process

	EDC	**SRDC**
N_T	41	20
D (m)	0.76	0.81
H (m)	28.53	13.17
Q_r (MW)	1.4129	1.0611
A_r (m2)	61.62	29.60
Q_c (MW)	0.8835	0.8300
A_c (m2)	25.80	16.75
Q_{cooler} (MW)	0.51	-
A_{cooler}(m2)	7.77	-
Total H.E. cost (10^6 $)	0.1943	0.1116
Column shell cost (10^6 $)	0.1935	0.1114
Total capital (10^6 $)	0.3877	0.2229
Cost of energy ($/GJ)	8.22	9.88
Operating cost (10^6 $/yr)	0.3663	0.3306
payback period (yr)	3	3
TAC (10^6 $ /yr)	0.4955	0.4049
Total capital cost (10^6 $)	0.6106	
Total operating cost (10^6 $/yr)	0.6969	
Total TAC (10^6 $ /yr)	0.9004	

3. PRESSURE-SWING DISTILLATION

Pressure Swing Distillation (PSD) process was designed for separating an azeotropic mixture of IPA and water using Aspen Plus. A simulation model was developed by using RADFRAC block and NRTL property method based on the vapor-liquid equilibrium data of the binary system.

Fig. 5(a) gives Txy diagram for the IPA-water system at two different pressures. At 1 atm, the azeotropic composition is 67.28 mol% IPA and the temperature is 80.18 C. At 12 atm, the azeotropic composition is 60.35 mol% IPA and the temperature is 160.22 C. This smaller shift in azeotropic composition is also clearly shown in the Fig.2 (b). It indicates that pressure swing distillation may not be attractive for this system. The purpose of this paper is to explore quantitatively this problem

3.1 Selection of Pressure

The pressures in the two columns are selected by finding the effect of pressure on the two azeotropic compositions and on the temperatures in the reboilers. The larger difference in the pressure, the larger the shift in the azeotropic composition and resulting the lower the recycle flow rates and energy consumption (Luyben, 2013).

The pressure in the low pressure column (LPC) is selected such that the reflux temperature is high enough to permit the use of cooling water in the condenser. The pressure in the high pressure column (HPC) is selected such that high pressure steam can be used in the reboiler.

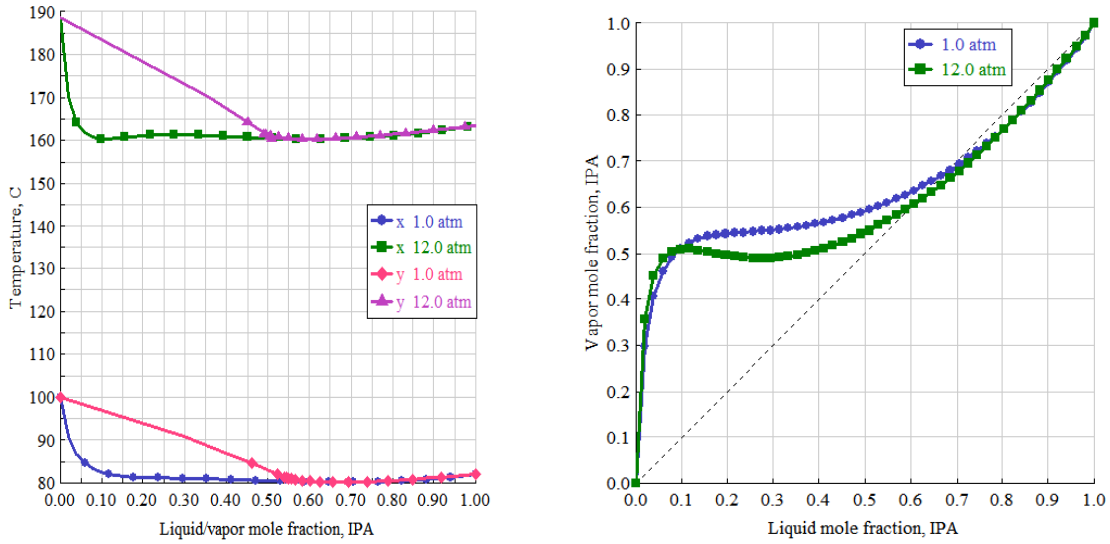

(a) (b)

Fig.5 (a) Txy diagram **(b)** xy diagram IPA Water system at 1atm and 12 atm.

3.2 Selection of Recycle flow rate

When the feed contains 50 mol% IPA and 50 mol % water, the PSD process was carried out with a column sequence of LP-HP, in which the low and high pressures are set at 1 atm and 12 atm, respectively in both columns. In the LPC, the water product is produced at the bottom and the corresponding top product is the azeotrope of IPA and water. On the other hand, the IPA product is obtained at the bottom if an HPC is used and the top product is the azeotrope of IPA and water.

The feed composition (z = 50 mol% IPA) and flow rate (F = 100 kmol/h) are taken, as well as the desired compositions of the two product streams B_1 at x_{B1} = 99.9 mol% water and streams B_2 at x_{B2} = 99.9 mol% IPA. Overall and component balance gives the flow rates of the two product streams.

$F = B_1 + B_2$

$zF = B_1x_{B1} + B_2x_{B2}$

Substituting the known numerical values gives,

$100 = B_1 + B_2$

$(0.5)(100) = B_1 (0.999) + B_2 (0.001) \Rightarrow B_1 = B_2 = 50$ kmol/h

The compositions of the two distillate streams are selected to be close to the two azeotropic compositions at the two pressures. For the low pressure column, the distillate composition must be slightly lower than or equal to azeotropic composition value. Suppose we select x_{D1} = 66.28 mol% IPA. For the high-pressure column, the distillation composition must be slightly higher than or equal to azeotropic composition value. Suppose we select x_{D2} = 61.35 mol% IPA, then total and component balances around the second column give the flow rates of the two distillate recycle streams.

$D_1 = D_2 + B_2$

$D_1x_{D_1} = D_2xD_2 + B_2xB_2$

The recycle stream D_2 from the high pressure column back to the low pressure column can be solved for.

$D_2 = B_2 (x_{B2} – x_{D1}) / (x_{D1} – x_{D2})$

This equation clearly shows the strong dependence of the recycle flow on the difference between the two distillate compositions. Substituting the known numerical values gives,

$D_1 = D_2 + 50$

$D_1 (0.6628) = D_2 (0.6135) + B_2 (0.999)$

$\Rightarrow \quad D_2 = 340.97$ kmol/h

$D_1 = 390.97$ kmol/h

Starting with this initial estimate of the D_2 recycle, simulations were run, to find the recycle that minimized reboiler heat input in the high pressure column. The optimum D_2 flow rate is 235.77 kmol/h. The resulting recycle compositions are x D_1 = 67.27 mol% IPA and xD_2 = 60.35 mol% IPA, which are slightly further from the azeotropic compositions than the initial guesses.

3.3 Aspen simulation

The two columns (LPC and HPC) are simulated in Aspen Plus using rigorous Radfrac models. The NRTL physical property package is used. The two bottom flow rates are fixed at 50 kmol/h and an Aspen Design/Spec Vary is set up in each column to drive the bottom compositions to their corresponding purity specifications by varying the reflux ratios. The separation in the low pressure column (LPC) is easy, so a 40-stage column is selected. The difficult separation is in the high pressure column. Columns with different numbers of stages were explored and the optimum was selected on the basis of minimum reboiler and condenser duty.

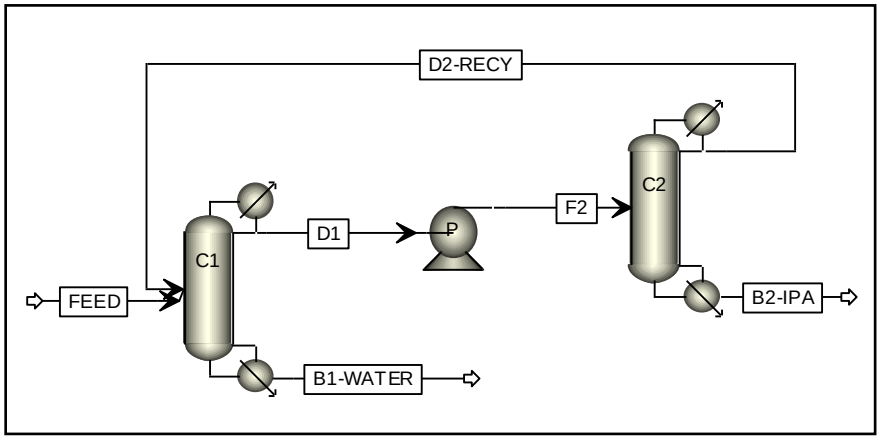

Fig.6 Flowsheet for the pressure swing distillation of IPA water system.

The process flow sheet for this separation system can be seen in Fig.6, the fresh feed (FF) combines with the distillate from the pressurized column (D2) which is the feed point (FF + D2). It is separated into pure water at the bottom of the atmospheric distillation column. The top of the atmospheric distillation column is close to azeotropic composition and is send to the pressurized column. The stream from the bottom of the high pressure column (B_2) is IPA with high purity and the distillate (D2) is recycled back to the atmospheric distillation column.

A distillation column has some design degrees of freedom when the feed and pressure have been fixed, which includes the number of stages (NT), the feed stage location (NF), the bottom flow rate B, and the reflux ratio RR. Sensitivity analysis was performed of the above parameter to obtain the specified purity of the product with minimum energy consumption and results shown in table 8.

Table 8 Configuration of LPC and HPC of pressure swing distillation system

Parameter	LPC	HPC
Number of stages	40	60
Feed stage	33	35
Molar reflux ratio	3	5
Condenser	total	total
Pressure (atm)	1	12
Bottom flow Rate(kmol /h)	50	50

Table 9 Simulation Results for complete process flow-diagram for Pressure swing distillation of IPA Water system

Stream Name	Temperature(°C)	Total mole flow (kmol / h)	IPA(mole fraction)	Water(mole fraction)
FEED	25.00	100.00	0.5000	0.5000
D1	80.18	285.79	0.6727	0.3273
B1-WATER	99.27	50.00	0.0010	0.9990
F2	80.97	285.79	0.6727	0.3273
D2-RECY	160.22	235.79	0.6036	0.3964
B2-IPA	163.37	50.00	0.9990	0.0010

Table 10 Condenser and Reboiler Heat Duties on the Columns

	LPC	HPC
Condenser (MW)	12.462	12.6010
Reboiler (MW)	11.7162	13.8717

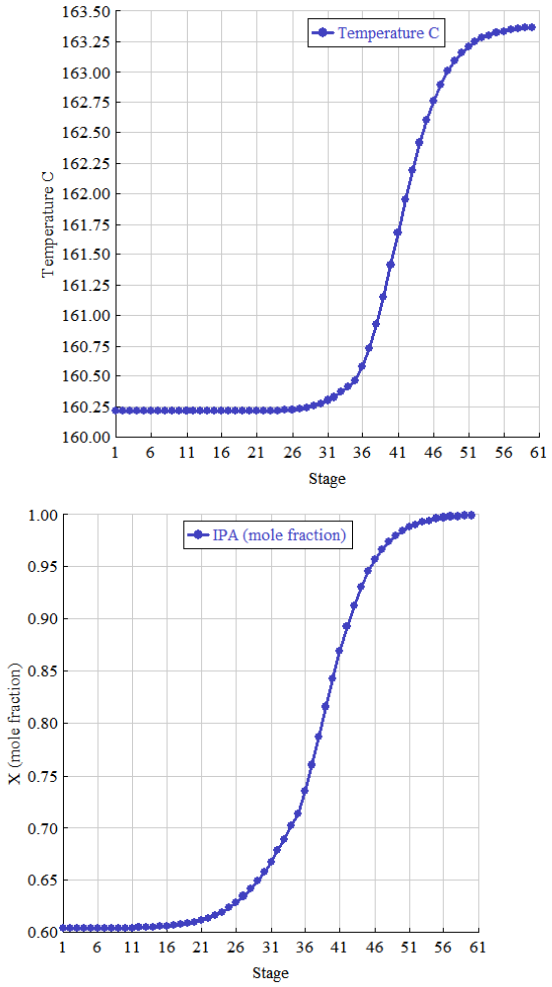

(a) (b)

Fig.7 (a) Temperature and **(b)** composition profile of high pressure column

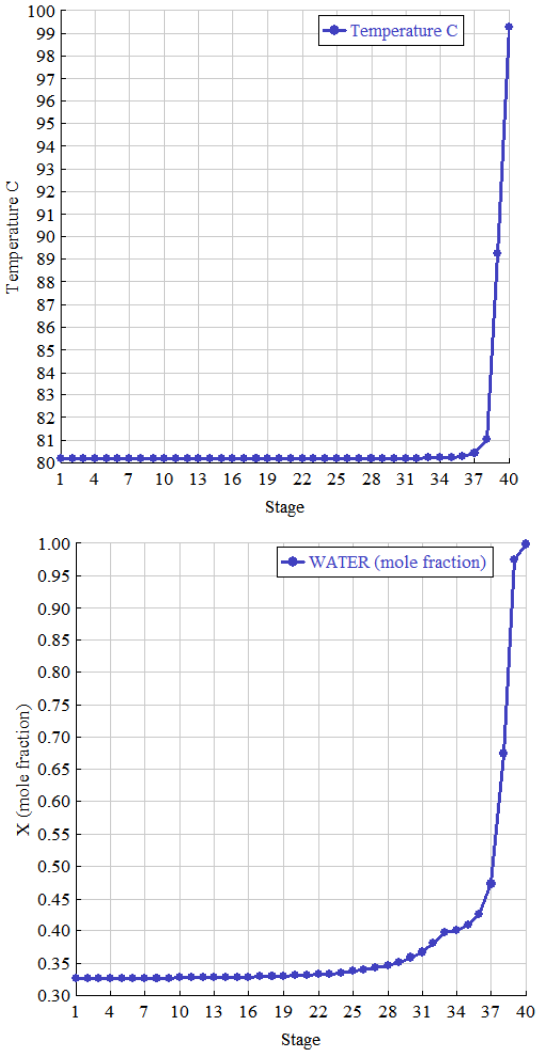

(a) (b)

Fig.8 (a) Temperature and **(b)** composition profile of low pressure column

3.4 Economic Analysis

Complete economic analysis of pressure swing distillation system was done similarly like the extractive distillation system. The basis of economics and equipment sizing relationships used, which were proposed by Luyben (2013). Table 11 gives TAC of pressure swing distillation sequence. Total capital investment was estimated to be $\$2.5718\times10^6$. Annual energy cost was 7.3592×10^6 \$ per year, using medium pressure steam in the reboiler of the LPC and high pressure steam in the reboiler of the second column.

Table 11 TAC of Pressure swing distillation process

	LPC	**HPC**
NT	40	60
D (m)	2.54	2.36
H (m)	27.797	42.427
Qr (MW)	11.7162	13.8717
Ar (m^2)	243.89	269.91
Qc (MW)	12.4630	12.601
Ac (m^2)	302.67	115.22
Total H.E. cost (10^6 $)	0.5589	0.4372
Column shell cost (10^6 $)	0.6857	0.89
Total capital (10^6 $)	303.23	115.65
Cost of energy ($/GJ)	8.22	9.88
Operating cost (10^6 $/yr)	3.0372	4.3221
payback period (yr)	3	3
TAC (10^6 $ /yr)	3.452	4.7645
Total capital cost (10^6 $)	2.5718	
Total operating cost (10^6 $/yr)	7.3592	
Total TAC (10^6 $ /yr)	8.2165	

5. PROCESS COMPARISONS

In this section, we will make a comparison between Pressure swing distillation and extractive distillation system simulated. The optimal results are shown in table 12. It is cleared from the results that Extractive distillation is more feasible than pressure swing distillation for the separation of the IPA -Water azeotropic mixture.

Table 12 Comparison of extractive distillation and pressure swing distillation

Parameter	**Extractive distillation**	**Pressure swing distillation**
Nt_1	41	40
Nt_2	12	60
QR1 (kW)	1.4129	11716.2
QR2 (kW)	1.0611	13871.7
Total TAC (10^6 $ /yr)	0.9004	8.2165

6. CONCLUSION

When the purities of the two product streams are set at specified value, it is revealed that the extractive distillation process is significantly more attractive from the standpoint of view of both economical and energy consumption as compared to the pressure-swing distillation. But pressure-swing distillation avoids the potential problem

of product contamination due to the extractive solvent that must be added to the binary system.

REFERENCES

[1] Chien I-L, Zeng KL, Chao HY. Design and control of a complete heterogeneous azeotropic distillation column system. Ind Eng Chem Res 2004; 43: 2160-2174.

[2] Cho J, Jeon JK. Optimization study on the azeotropic distillation process for isopropyl alcohol dehydration. Korean J Chem Eng 2006; 23: 1-7.

[3] Doherty MF, Malone MF. Conceptual design of distillation systems. New York, USA: McGraw-Hill; 2001.

[4] Luyben WL, Chien I-L. Design and control of distillation systems for separating azeotropes. John Wiley & Sons; 2011.

[5] Luyben WL. Comparison of extractive distillation and pressure-swing distillation for acetone/chloroform separation. Comput Chem Eng 2013; 50:1–7.

[6] Yuan S , Zou C, Yin H, Chen Z, Yang W. Study on the separation of binary azeotropic mixtures by continuous extractive distillation. Chem Eng Res Des 2015; 93:113-119.

State-based feedback control of a two qubit quantum system in the presence of time delays

A. A. Vhatkar and P. M. Shevgaonkar*

Chemical Engineering Department, Vishwakarma Institute of Technology, Pune 411037, India

Abstract

Feedback control of a quantum system can be significantly affected by the presence of time delays. We examine the effect of time delays on the performance of state-based local feedback control of a two qubit quantum system. The quantum system undergoes continuous weak measurements of both qubits and is represented by the stochastic master equation. The control strategy involves constructing a feedback Hamiltonian at every simulation step, which rotates the estimated Bloch vectors of the two qubits towards the target states. We find that the strength of the feedback Hamiltonian needs to be limited to maintain stablility in the presence of time delays. The entanglement of the two qubits is maximized at a specific value of this limiting strength. The value of this maximum does not depend significantly on the extent of time delay. This, however, occurs at the cost of fidelity with respect to the target states. The speedup in the rate of state purification is marginal in the presence of time delays.

1 Introduction

The field of quantum control, which has evolved over the last 30 years, has been truly multidisciplinary in nature, with inputs not only from pure sciences but also from the engineering communities [1]. In quantum control at least one component of the control system, typically the system being controlled, exhibits explicit quantum mechanical behavior.

A key difference between classical and quantum measurements is that even an ideal quantum measurement can affect the state of a quantum system. Amongst the main approaches to quantum control, the use of contiunous weak measurements to control the behaviour of quantum systems has been considered in a number of theoretical and experimental studies [1–8]. If a quantum system is weakly coupled to a 'meter' and repeated measurements are carried out on the meter, a 'continuous weak measurement' results in the limit. The evolution of the state of the quantum system conditioned on such continous weak measurements is termed as quantum filtering [9]. The resulting model describing the nonunitary evolution of the system state is called a Quantum Stochastic Master Equation (SME).

The use of classical weak measurement signals to device a feedback control scheme for control of quantum systems is referred to as measurement-based quantum feedback control (MFC) or incoherent quantum feedback control [1, 10]. Within MFC, control could be achieved with minimal computational efforts by using a feedback Hamiltonian which is simply a functional of the measurement signal. Altenatively, an estimate of the conditional density matrix representing the state of the system could be made using SME and the feedback scheme could be based on this state estimate. This approach is called state-based or Bayesian feedback control [1, 2].

Two of the applications of quantum control are rapid purification and entanglement control. In rapid purification, measurement-based feedback control is used to increase the rate of purification of the state of a quantum system from an initial mixed state [11]. A speedup of a factor of two can be achieved using this scheme. The second important application of quantum control involves control of quantum entanglement. In one of the approaches it was shown that entanglement between two qubits can also be controlled to some extent by use of local controls, ie without direct control of the entangling interaction itself [12–14].

*Email: prashant.shevgaonkar@vit.edu

As in classical control, an important parameter which can affect the performance of a quantum control system is time delay or dead time in measurements [15–17]. The presence of measurement time delay can severely degrade the performance of a quantum control system, possibly causing instability [17].

In this paper, we study the effects of time delay on a simulated two qubit quantum system under state-based feedback control. The control objectives of interest are the rate of state purification and the extent of entanglement achieved.

2 Quantum Control System

2.1 Stochastic Master Equation

We consider a two-qubit quantum system undergoing continuous weak measurements described by the Stochastic Master Equation:

$$\begin{aligned} d\rho = &- i[H,\rho]dt \\ &+ \sum_{r=1}^{2}\Big\{L_r\rho L_r^\dagger - \frac{1}{2}L_r^\dagger L_r\rho + \rho L_r^\dagger L_r\Big\}dt \\ &+ \sum_{r=1}^{2}\sqrt{\eta_r}\Big\{L_r\rho + \rho L_r^\dagger - Tr(L_r\rho + \rho L_r^\dagger)\Big\}dW_r \end{aligned} \tag{1}$$

Here ρ is the 4x4 conditional density matrix of the two qubit system, t is time and dW_r represents Wiener increments. The total Hamiltonian H is given by

$$H = H_s + H_{fb} \tag{2}$$

where H_s represents the system Hamiltonian without control, whereas H_{fb} is the applied feedback control Hamiltonian.
We consider a system Hamiltonian containing only an interaction term of the form

$$H_s = \kappa(ZZ) \tag{3}$$

where Z is the Pauli spin matrix and κ is the strength of the interaction between the two qubits. Terms like ZZ indicate tensor product.
The two qubits are measured in their respective Z bases. Thus the two measurement operators are:

$$L_1 = \sqrt{2k_1}(ZI) \tag{4}$$

$$L_2 = \sqrt{2k_2}(IZ) \tag{5}$$

Here k_1 and k_2 are the measurement strenghts and I is the 2x2 identity operator. We use $\kappa = 0.01\omega_0$ and $k_1 = k_2 = 0.001\omega_0$, where ω_0 indicates a reference oscillation frequency, taken as 1 in the simulation. The measurement efficiency η_r is taken as 1. Feedback control is achieved by manipulating the feeback Hamiltonian H_{fb} at each simulation step as explained in the next section.

2.2 Numerical Simulation of the SME

The numerical method we have used for the simulation of the SME (1) is a modification of the Euler-Milstein method [18] proposed by Rouchon and Ralph [10]. This method, reminiscent of the Joseph form of Kalman filter [19], makes use of a form that maintains the positivity of the density matrix. Under this numerical scheme, increment to the density matrix ρ in a simulation time interval Δt is given as follows:

$$\rho(n+1) = \frac{S(n)}{Tr(S(n))} \tag{6}$$

$$S(n) = M_n\rho(n)M_n^\dagger + \sum_{r=1}^{2}(1-\eta_r)L_r\rho(n)L_r^\dagger\Delta t \tag{7}$$

The operator M_n is given by

$$M_n = I - \Big(iH + \frac{1}{2}\sum_{r=1}^{2} L_r^\dagger L_r\Big)\Delta t + \sum_{r=1}^{2}\sqrt{\eta_r}L_r\Delta y_r(n) + \sum_{r,s=1}^{2}\frac{\sqrt{\eta_r\eta_s}}{2}L_rL_s(\Delta y_r(n)\Delta y_s(n) - \delta_{r,s}\Delta t) \quad (8)$$

The measurement increments in the above expression are given by

$$\Delta y_r(n) = \sqrt{\eta_r}Tr(L_r\rho(n) + \rho(n)L_r^\dagger)\Delta t + \Delta W_r(n) \quad (9)$$

The Wiener increments are generated at every step using a random number generator for normal distribution with zero mean and a variance of Δt.

2.3 The Control Algorithm

In the implementation of quantum control in the presence of time delays, we have used a target state (setpoint) corresponding to the y-direction of the Bloch sphere representation of each qubit. The local control actions then involve rotating the Bloch vector of each qubit towards the target vector in each simulation step. This is achieved by implementing an appropriate feedback Hamiltonian, H_{fb} (see (1),(2)). The parameters of the system and the estimator are assumed to be identical. Therefore separate simulations for the system and the estimator are not needed. The steps involved in the computation of the control Hamiltonian are explained below for qubit A. Computations for qubit B are on similar lines.

1. Calculate $\rho(n+1)$ using (6).
2. Find the reduced density matrx ρ_A. For this use the past value of density matrix based on the time delay.
3. Find the Bloch vector $\mathbf{n_A}$ from the reduced density matrix.
4. From $\mathbf{n_A}$ and $\mathbf{n_{A,SP}}$, the target vector, find the unit vector $\mathbf{n_{A,fb}}$ representing the rotation axis.
5. Find the required angle of rotation $\theta_{A,fb}$.
6. Based on $\mathbf{n_{A,fb}}$ and $\theta_{A,fb}$, calculate the feedback control Hamiltonian corresponding to local rotations of qubit A as
$$H_{A,fb} = \frac{\omega_{A,fb}\Delta t}{2}(\mathbf{n_{A,fb}}\cdot\boldsymbol{\sigma})\otimes I \quad (10)$$
where the Pauli vector is given by
$$\boldsymbol{\sigma} = \hat{\mathbf{x}}X + \hat{\mathbf{y}}Y + \hat{\mathbf{z}}Z \quad (11)$$
The feedback rotation frequency, ω_{fb}, is given for quabit A by $\omega_{A,fb} = \theta_{A,fb}/\Delta t$. At high values of this parameter, the control system becomes unstable in the presence of time delays as explained further in the results and discussion section. Therefore, this value is restricted to an upper limit ω_m during a particular simulation step as follows:
$$if \quad \omega_{A,fb} \geq \omega_m, \quad \omega_{A,fb} = \omega_m \quad (12)$$
7. Finally, calculate the total feedback Hamiltonian
$$H_{fb} = H_{A,fb} + H_{B,fb} \quad (13)$$

The numerical simulation uses 5000 steps per reference rotation period $T = 2\pi/\omega_0$. Thus here, the simulation step interval Δt is $2\pi/5000$. For finding ensemble averages, 100 realizations are used. Hereafter, parameters with units of time such as time delay τ_d, time constant τ refer to dimensionless values with respect to the charactersitic time, T.

2.4 Performance Measures

Various performance measures used to envaluate the performance of the control system are as follows:

2.4.1 Purity

To estimate the extent of mixedness of the two qubit system, we use purity given by

$$P = Tr(\rho^2) \tag{14}$$

For a pure quantum state of the two-qubit system under consideration, purity is 1 and for a completely mixed state it is 0.25.

2.4.2 Concurrence

The extent of entanglement of the two qubits is estimated using concurrence. For a two qubit system, concurrence is given by [20, 21]

$$C(\rho) = max(0, \sqrt{\lambda_1} - \sqrt{\lambda_2} - \sqrt{\lambda_3} - \sqrt{\lambda_4})$$

where $\sqrt{\lambda_1}...\sqrt{\lambda_4}$ are eigenvalues of the matrix $\rho(YY)\rho^*(YY)$ in non-increasing order. ρ^* is the complex conjugate of ρ. Concurrence for an unentangled state of two qubits is zero, whereas for a maximally entangled pure state it is 1.

2.4.3 Quantum Angle

Proximity of each qubit to the target state is estimated using the expression $2\theta_{QA}$, where θ_{QA} is the quantum angle estimated as follows [22]

$$\theta_{QA} = cos^{-1}(\sqrt{F}) \tag{15}$$

where the Fidelity, F is given by

$$F(\rho_1, \rho_2) = \left| Tr\left(\sqrt{\sqrt{\rho_1}\rho_2\sqrt{\rho_1}}\right)\right|^2 \tag{16}$$

The quantum angle gives a rough indication of proximity to the target state. For example, the steady state of both qubits in the absence of control is along the Bloch z-axis. The quantum angle, θ_{QA} wrt to the target y-axis state then is 45^o, so that $2\theta_{QA}$ gives the actual angle of 90^o. Of course, a mixed state along y-axis does give a non-zero quantum angle and thus this is not a direct measure of proximity to the target state. However, for similar mixedness, this parameter should give an indication of the extent to which the control at target state has been achieved.

3 Results and Discussion

We carried out simulation runs for different values of the measurement time delay, τ_d. Each run used a specific maximum value of the frequency ω_m used to rotate the individual qubit Bloch vectors onto the target vectors as explained in (12) above. Simulation runs were also carried out in the absence of control for comparison. The total simulation time was 50. The initial state used was the completely mixed state unless otherwise specified. For finding ensemble means, 100 realizations were used.

Figure 1 shows the system dynamics in the absence of control for a single realization. As expected, the two qubits approach the z-axis on the Bloch sphere at the end of a random walk, settling down into one of the four possible configurations of spin up/down states. The steady-state length of the Bloch vectors is unity. Thus the two-qubit system evolves into a pure state with no entanglement, ie with zero concurrence. The time constant of this evolution is 6.2.

Feedback contol simulation results for the case of $\tau_d = 0.05$ are shown in Figure 2. As the ω_m value is lowered from 2.5, the steady state average concurrence increases from about 0.12 to 0.43, approaching the theoretical limit of 0.45 [10]. A further reduction in ω_m reduces the concurrence. At $\omega_m = 0.05$ it is 0.32. The limit of $\omega_m = 0$ indicates no control, so the concurrence tends to zero in this limit.

As shown in Figure 2(b), the parameter $2\theta_{QA,A}$ is at a minimum of 21^o at $\omega_m = 1.5$. At high ω_m the system becomes unstable in the presence of time delay resulting in a high quantum angle. Moreover, the entanglement also vanishes, indicated by concurrence approaching zero. Similarly, at low ω_m the control becomes weak causing a pull towards the Bloch z-axis and thus $2\theta_{QA}$ increase.

Bloch plot of a single realization of the control system for the case of $\tau_d = 0.05$ and $\omega_m = 0.5$ is shown in Figure 3. The Bloch vectors starting off from the origin, show an initial overshoot and then evolve

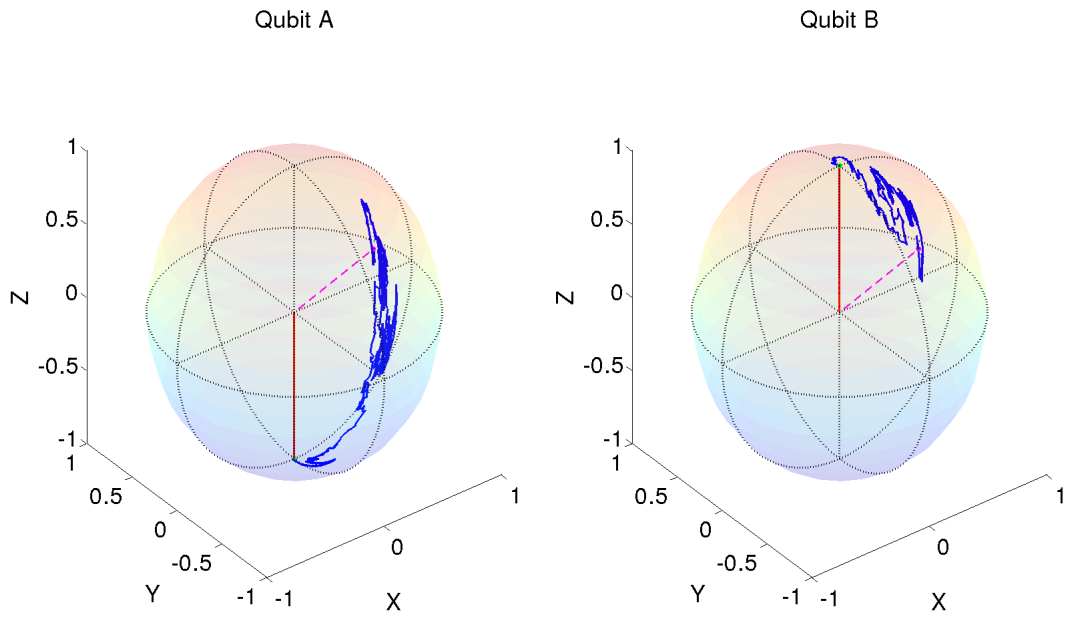

Figure 1: Plots of a single realization of the evolution of the states of the two system qubits on Bloch spheres. No control is applied. Dashed lines indicate the initial states. Solid lines indicate the final states of the qubits at the end of the simulation time of 50.

towards the target state $\hat{y}$. The low value of ω_m causes the trajectory to exhibit random oscillations around the target state as indicated by the smeared out blob. Since the concurrence in this case is high (0.43), the Bloch vectors do not reach the surface of the Bloch sphere.

The time constant for the purity dynamics in this case is 5.03, which is about 20% less than the value without control, 6.2. Thus, as expected, the speed of purification is better than the no control case, but worse than the case of no time delay. The value of the time constant for no time delay case with no limit on ω_{fb} is 4.9.

Table 4 shows the maximum values of concurrence with respect to time delay obtained during the simulation runs of the control system at steady state. The maximum concurrence achieved decreases with increasing time delay, but the reduction is not too drastic. The ω_m values which yield maximum concurrence decrease with increase in time delay. The quantum angle $\theta_{QA,Q}$ increases with time delay, thus indicating that the final quantum state is bound to show lower fidelity. However, the lower concurrence contributes to this increase in the quantum angle. Thus around these ω_m values, the control system performance in terms of proximity to the target y-axis is not too sensitive to ω_m.

4 Conclusions

In this paper, we have studied the effect of time delay on the performance of a simulated state-based quantum control system composed of two qubits under the influence of an interaction Hamiltonian. Both the qubits are measured in the Z-basis. The state-based controller acts on past states of the system due to the presence of time delays. The controls are local. The target state for each qubit is the unit Bloch vector along the y-axis. The feedback Hamiltonian strength ω_{fb} is restricted to a limiting value of ω_m to maintain stability. We find that for a fixed time delay, the concurrence shows a maximum close to the theoretical value of 0.45 as a function of ω_m. This maximum concurrence shows modest decrease with increasing time delay. At lower and higher values of ω_m, the concurrence drops to zero. The limit on the feedback strength coupled with the presence of time delay cause fluctuations in the quantum state around the target state. State purification dynamics is speeded up, but marginally so. These results suggest the possibility of achieving quantum entanglement closer to the theoretical maximum with proper tuning of the controller.

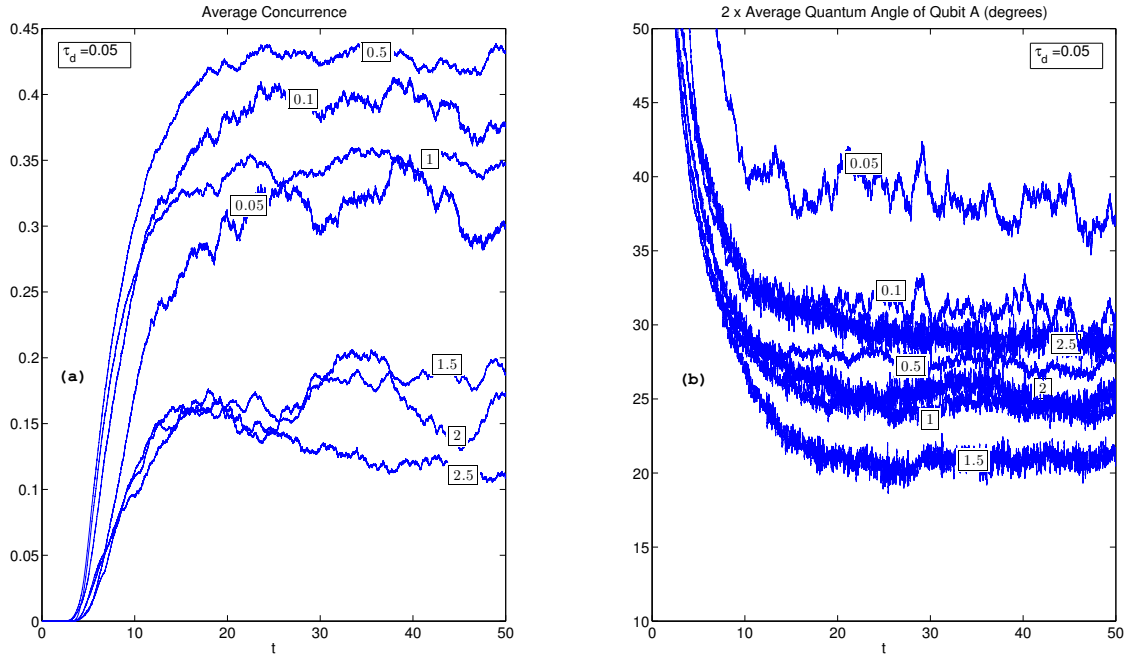

Figure 2: Simulation results for $\tau_d = 0.05$. System is under feedback control. The labels on the curves indicate values of the limiting feedback Hamiltonian rotation frequency ω_m used. t is dimensionless time. (a) Average Concurrence of the two qubits and (b) 2 x Average Quantum Angle of qubit A are averaged over 100 realizations. Quantum angle of qubit B shows similar trend.

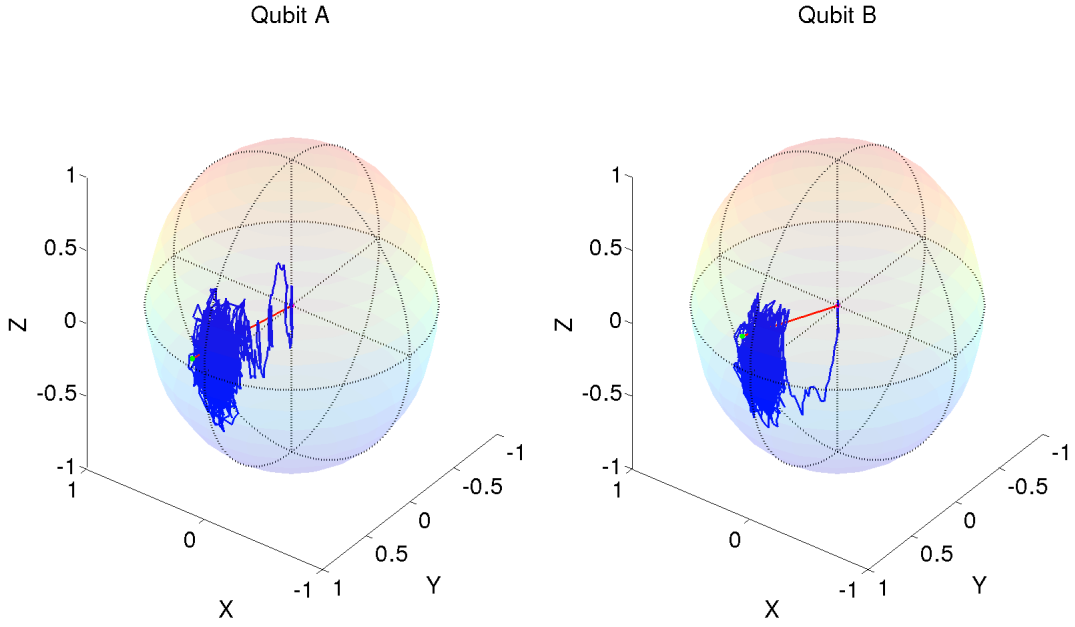

Figure 3: Bloch sphere plots of a single realization of the evolution of the states of the two system qubits under feedback control. Time delay is 0.05 and ω_m is 0.5. Target state is the unit Bloch vector $\hat{\mathbf{y}}$. The initial state is fully mixed, starting at the origin. Solid lines indicate the final states of the qubits at the end of the simulation time of 50.

τ_d	ω_m	C	$2\theta_{QA,A}$
0	0.5	0.44	26.5
0.01	0.7	0.44	26.5
0.05	0.5	0.43	27.3
0.1	0.4	0.42	28.6
0.15	0.3	0.41	29.6
0.20	0.2	0.40	30.5
0.30	0.2	0.38	32.6

Table 1: Concurrence C and $2\theta_{QA,A}$ where $\theta_{QA,A}$ is the quantum angle for qubit A, for various time delay values τ_d. The values reported are for maximum steady state concurrence obtained for a given time delay. ω_m indicates the limiting feedback rotation frequency used.

References

[1] J. Zhang, Y.-x. Liu, R.-B. Wu, K. Jacobs, and F. Nori, "Quantum feedback: theory, experiments, and applications," *arXiv:1407.8536*, July 2014.

[2] H. Wiseman and G. Milburn, *Quantum Measurement and Control*. Cambridge University Press, 2010.

[3] M. A. Armen, J. K. Au, J. K. Stockton, A. C. Doherty, and H. Mabuchi, "Adaptive Homodyne Measurement of Optical Phase," *Physical Review Letters*, vol. 89, p. 133602, Sept. 2002.

[4] C. Sayrin, I. Dotsenko, X. Zhou, B. Peaudecerf, T. Rybarczyk, S. Gleyzes, P. Rouchon, M. Mirrahimi, H. Amini, M. Brune, J.-M. Raimond, and S. Haroche, "Real-time quantum feedback prepares and stabilizes photon number states," *Nature*, vol. 477, pp. 73–77, Sept. 2011.

[5] R. Vijay, C. Macklin, D. H. Slichter, S. J. Weber, K. W. Murch, R. Naik, A. N. Korotkov, and I. Siddiqi, "Stabilizing Rabi oscillations in a superconducting qubit using quantum feedback," *Nature*, vol. 490, pp. 77–80, Oct. 2012.

[6] M. S. Blok, C. Bonato, M. L. Markham, D. J. Twitchen, V. V. Dobrovitski, and R. Hanson, "Manipulating a qubit through the backaction of sequential partial measurements and real-time feedback," *Nature Physics*, vol. 10, pp. 189–193, Mar. 2014.

[7] K. W. Murch, S. J. Weber, C. Macklin, and I. Siddiqi, "Observing single quantum trajectories of a superconducting quantum bit," *Nature*, vol. 502, pp. 211–214, Oct. 2013.

[8] S. J. Weber, A. Chantasri, J. Dressel, A. N. Jordan, K. W. Murch, and I. Siddiqi, "Mapping the optimal route between two quantum states," *Nature*, vol. 511, pp. 570–573, July 2014.

[9] V. P. Belavkin, "Quantum filtering of Markov signals on a background of white quantum noise," *Radiotekhnika i Elektronika*, vol. 25, pp. 1445–1453, July 1980.

[10] P. Rouchon and J. F. Ralph, "Efficient quantum filtering for quantum feedback control," *Phys. Rev. A*, vol. 91, p. 012118, Jan 2015.

[11] K. Jacobs, "How to project qubits faster using quantum feedback," *Phys. Rev. A*, vol. 67, p. 030301, Mar. 2003.

[12] A. R. R. Carvalho and J. J. Hope, "Stabilizing entanglement by quantum-jump-based feedback," *Phys. Rev. A*, vol. 76, p. 010301, July 2007.

[13] A. R. R. Carvalho, A. J. S. Reid, and J. J. Hope, "Controlling entanglement by direct quantum feedback," *Phys. Rev. A*, vol. 78, p. 012334, July 2008.

[14] E. Mascarenhas, B. Marques, M. T. Cunha, and M. F. Santos, "Continuous quantum error correction through local operations," *Phys. Rev. A*, vol. 82, p. 032327, Sept. 2010.

[15] S. S. Ge, T. Vu, and T. H. Lee, "Quantum measurement-based feedback control: A nonsmooth time delay control approach," *SIAM J. Control and Optimization*, vol. 50, no. 2, pp. 845–863, 2012.

[16] K. Kashima and N. Yamamoto, "Control of quantum systems despite feedback delay," *IEEE Transactions on Automatic Control*, vol. 54, no. 4, pp. 876–881, 2009.

[17] S. Wang and M. R. James, "Quantum feedback control of linear stochastic systems with feedback-loop time delays," *Automatica*, vol. 52, pp. 277–282, 2015.

[18] G. N. Milstein and M. V. Tretyakov, *Numerical Integration of Stochastic Differential Equations*. Springer, 1995.

[19] P. S. Maybeck, *Stochastic Models, Estimation and Control: Volume 1*. Academic Press, 1979.

[20] W. K. Wootters, "Entanglement of Formation of an Arbitrary State of Two Qubits," *Physical Review Letters*, vol. 80, pp. 2245–2248, Mar. 1998.

[21] N. A. Peters, T.-C. Wei, and P. G. Kwiat, "Mixed-state sensitivity of several quantum-information benchmarks," *Phys. Rev. A*, vol. 70, p. 052309, Nov. 2004.

[22] M. A. Nielsen and I. L. Chuang, *Quantum Computation and Quantum Information: 10th Anniversary Edition*. Cambridge University Press, 2011.